AGU ADVANCING EARTH AND SPACE SCIENCE

JGR Earth Surface

RESEARCH ARTICLE

10.1029/2021JF006221

Key Points:

- We apply the cosmogenic nuclide ^{10}Be(meteoric) and its ratio to ^{9}Be in one of the world's fastest-eroding basin
- ^{10}Be(meteoric)/^{9}Be ratios record extremely high denudation rates (>10 mm/yr)
- A soil-bedrock mixing model reveals that bedrock landslides are the cause of the high denudation rates

Supporting Information:

Supporting Information may be found in the online version of this article.

Correspondence to:

K. Deng,
103459@tongji.edu.cn

Citation:

Deng, K., Wittmann, H., Yang, S., & von Blanckenburg, F. (2021). The upper limit of denudation rate measurement from cosmogenic ^{10}Be(meteoric)/^{9}Be ratios in Taiwan. *Journal of Geophysical Research: Earth Surface*, *126*, e2021JF006221. https://doi.org/10.1029/2021JF006221

Received 17 APR 2021
Accepted 30 SEP 2021

The Upper Limit of Denudation Rate Measurement From Cosmogenic ^{10}Be(Meteoric)/^{9}Be Ratios in Taiwan

Kai Deng[1,2,3], Hella Wittmann[1], Shouye Yang[2], and Friedhelm von Blanckenburg[1,4]

[1]GFZ German Research Centre for Geosciences, Earth Surface Geochemistry, Potsdam, Germany, [2]State Key Laboratory of Marine Geology, Tongji University, Shanghai, China, [3]Institute of Geochemistry and Petrology, Department of Earth Sciences, ETH Zürich, Zürich, Switzerland, [4]Institute of Geological Sciences, Freie Universität Berlin, Berlin, Germany

Abstract The tectonically active Taiwan orogen features numerous rivers that yield a high amount of sediment with fluxes exceeding 10^4 t/km^2/yr. Amongst these, the landslide-dominated Liwu River is well studied regarding its dynamic surface processes. However, the quantification of denudation in the Liwu Basin is still an ongoing task as rates obtained to date are subject to substantial differences depending on methods that differ in their spatio-temporal scales. We constrain an upper limit of global denudation using the cosmogenic nuclide ^{10}Be(meteoric) and its ratio to stable ^{9}Be. Meteoric cosmogenic ^{10}Be is delivered to Earth's surface by precipitation, whereas stable ^{9}Be is released from rock weathering. In contrast to *in situ* cosmogenic ^{10}Be measured in quartz, the ^{10}Be(meteoric)/^{9}Be ratio can be analyzed in quartz-poor settings. ^{10}Be(meteoric)/^{9}Be-derived denudation rates (D_{met}) vary from 8.1 to >30 mm/yr in the Liwu mainstem, and from 3.4 to 21.5 mm/yr in the tributaries. These new D_{met} are among the highest cosmogenic nuclide-derived rates ever measured. Most of these rates agree with rates from sediment gauging or channel incision. We propose that stochastic landsliding plays a major role in denudation processes here. Using a soil-bedrock mixing model and published riverine organic ^{14}C data as a soil tracer, we estimate the fractional contribution of bedrock landslide material to mainstem sediments to be 55%–97%, which explains the magnitude and large variability (4-fold) in D_{met}. We demonstrate the complexity associated with denudation rates determination in landslide-dominated routing systems; but also the potential of ^{10}Be(meteoric)/^{9}Be for tracing stochastic landsliding processes.

Plain Language Summary Many of Earth's rivers that transfer sediments with an extremely high rate are found in the Taiwan mountain belt, where earthquakes and typhoons are very common. Determination of the sediment removal rate in these rivers is crucial for understanding of the evolution of mountain landscapes through time and their impact on ocean chemistry and atmospheric trace gases. We applied a denudation rate meter to river sediments from one of the fastest-eroding catchments in Taiwan, the Liwu River: the meteoric cosmogenic isotope beryllium-10 (^{10}Be) delivered by rainfall normalized to stable ^{9}Be. This geochemical tool is particularly suited for fast-eroding settings given the high delivery rate of meteoric ^{10}Be to Earth's surface. The measured ^{10}Be(meteoric)/^{9}Be-derived denudation rates in the Liwu Basin are highly variable and range from ~3 to >30 mm/yr. We find that stochastic bedrock landsliding is likely the cause for such magnitude and large variability in denudation. Liwu river sediments constitute a mixture between steadily eroding surface soil and bedrock materials released from depths that lack meteoric ^{10}Be. Our findings demonstrate the substantial potential of ^{10}Be(meteoric)/^{9}Be to trace sources of rainfall-triggered landslides.

1. Introduction

Tectonically active regions produce disproportionately high sediment (physical erosion) (Milliman & Syvitski, 1992) and dissolved (chemical weathering) (Gaillardet et al., 1999) fluxes to the oceans, and therefore play an important role in the global carbon cycle. As an active mountain belt, the Taiwan orogen alone bears eight of the world's 13 rivers with sediment yield >10^4 t/km^2/yr (Milliman & Farnsworth, 2011) that results from active tectonics and frequent typhoon events. Rates of mineral weathering from silicates and sulfides (Blattmann et al., 2019; Bufe et al., 2021) and rates of organic carbon transport and oxidation (Hemingway et al., 2018; Hilton et al., 2012) in the Taiwan orogen are among the highest worldwide as these processes are driven by rapid denudation. Hence, knowledge of denudation rates that integrate over time scales

Table 1
Sediment Flux ($\times 10^3$ t/km²/yr) in the Liwu River From Literature

Rate type	Method	Rate range	Data source
Suspended load	Gauging	33.1 ± 8.3	Dadson et al. (2003)
Channel incision	^{14}C or ^{36}Cl dating	16.7–68.9	Dadson et al. (2003) and Schaller et al. (2005)
Basin-averaged denudation	*In situ* ^{10}Be	2.1–13.2	Derrieux et al. (2014)
Basin-averaged exhumation	Fission-track dating	8.6 ± 2.1	Fellin et al. (2017)

characteristic of geologic processes is a prerequisite to quantifying the contribution of the Taiwan orogen to the global carbon cycle over 10^2–10^4 yrs timescales.

Among the small mountainous rivers in Taiwan, the landslide-dominated Liwu River (Kuo & Brierley, 2014), draining quartz-poor schist-slate and carbonate lithologies, is perhaps the best-studied. The Liwu River drains one of the fastest eroding catchments in Taiwan (Dadson et al., 2003; Derrieux et al., 2014; Fellin et al., 2017) and therefore has high carbon transfer rates that result from silicate weathering, sulfide oxidation driven carbonate dissolution, biospheric organic carbon transport-burial, and oxidation of petrogenic organic carbon (Calmels et al., 2011; Hemingway et al., 2018; Hilton et al., 2008; Hilton & West, 2020; Kao et al., 2014). Despite being a classic study site for rapidly eroding settings, the quantification of its denudation rate is still ongoing. Multiple techniques, including surveys of channel bedrock elevation using dated benchmarks (Hartshorn et al., 2002), sediment gauging (Dadson et al., 2003), dating incised terraces (Dadson et al., 2003; Schaller et al., 2005), *in situ* cosmogenic ^{10}Be in quartz from river sediment (Derrieux et al., 2014), and thermochronology (Fellin et al., 2017) have been employed in the Liwu River from local to basin scales and from single events to million-year timescales. A ∼30-fold variability in denudation rates emerged from these methods (Table 1).

In this study, we investigated denudation processes in the Liwu River using the ^{10}Be(meteoric)/^{9}Be ratio as a denudation rate proxy. Meteoric beryllium-10 (^{10}Be) is produced in the atmosphere and scavenged primarily by rainfall to the Earth's surface, while the release of stable ^{9}Be from bedrock depends on chemical weathering (Barg et al., 1997; von Blanckenburg et al., 2012). Unlike the sister nuclide *in situ* cosmogenic ^{10}Be produced in quartz at a rate of 10^0–10^2 atoms/g/yr, the ^{10}Be(meteoric)/^{9}Be system integrates all lithologies including quartz-poor rock types and only requires ∼1 g for analysis due to a much higher depositional flux (e.g., ∼10^6 atoms/cm²/yr) (Deng, Wittmann, & von Blanckenburg, 2020; von Blanckenburg et al., 2012). Hence, the ^{10}Be(meteoric)/^{9}Be ratio has been applied to track millennial-scale denudation processes in basins ranging from creek to continental-scale sizes (e.g., Dannhaus et al., 2018; Deng, Yang, et al., 2020; Portenga et al., 2019; Rahaman et al., 2017; Wittmann et al., 2015). In previous studies the denudation rates derived from *in situ* ^{10}Be and ^{10}Be(meteoric)/^{9}Be ratios mostly agreed within a factor of two. Where larger differences between both methods were found, their distinct response might be due to true variability in geologic conditions (e.g., lithology) and differences in denudation rate resulting thereof (Portenga et al., 2019; Wittmann et al., 2015).

By analyzing ^{10}Be(meteoric)/^{9}Be ratios of mainstem and major tributary sediment samples in the Liwu River, we constrain one of the world's highest denudation rates and show that stochastic landsliding is a plausible control on such extremely high and variable erosion rates. This study provides valuable insight into the applicability of cosmogenic nuclides in fast-eroding orogens.

2. Study Area

Collision between the Luzon Arc and the Asian continental margin has driven rapid uplift of the Taiwan orogen since ∼6 Ma (Huang et al., 2006). Six tectonic units are exposed from west to east: the Coastal Plain, Western Foothills, Hsuehshan Range, Backbone Range, Tananao Metamorphic Complex (Tailuko Belt and Yuli Belt) and Coastal Range (Figure 1a). The Backbone Range and the Tananao Complex can be grouped together as the Central Range. The island as a whole is mainly composed of (meta-) sedimentary rocks ranging in age from Paleozoic to Quaternary. The Liwu River, located at the eastern side of the mountain belt, drains the Miocene and Eocene slate of the Backbone Range in the headwaters, and then flows across

10.1029/2021JF006221

Table 2
Basin Metrics and Lithological and Sediment Descriptions for Sampling Locations[a]

Sampling location[b]	Catchment	Upstream distance from river mouth (km)	Longitude (°E)	Latitude (°N)	Area (km^2)	Mean slope (m/m)	Mean precipitation rate[c] (m/yr)
WH	Waheir	25.3	121.486	24.185	57	0.70	3.2
DS	Dasha	23.2	121.498	24.180	184	0.70	3.0
LW3[d]	Liwu	23.2	121.498	24.180	433	0.70	3.2
LW2	Liwu	13.0	121.582	24.173	512	0.70	3.1
SKD	Shakadang	7.8	121.612	24.165	61	0.80	2.7
LW1	Liwu	5.4	121.628	24.154	609	0.70	3.0

Sampling location	Miocene slate (%)	Eocene slate (%)	Tailuko (schist, %)	Tailuko (marble, %)	Sediment description (sample no.)[e]
WH	4	39	58	0	WH-2: medium sand; WH-3: very fine sand; both near water line
DS	0	27	73	0	DS-2: medium sand above water line; DS-3: very coarse silt on bedrock from a higher position, suggesting a flood deposit
LW3	6	26	62	7	LW3-1: very coarse silt; LW3-2: coarse silt; both near water line
LW2	5	22	60	13	LW2-1: fine sand; LW2-2: very coarse silt; both near water line
SKD	0	0	40	60	SKD-2: very fine sand near water line
LW1	4	18	56	22	LW1-1, LW1-2: coarse silt sampled in floodplain

[a]The basin metrics were extracted using the MATLAB-based software TopoToolbox 2 (Schwanghart & Scherler, 2014). [b]The samples are sorted according to the upstream distance from the river mouth. [c]The basin-averaged annual precipitation data set (with an observation period of 1970–2000) is sourced from WorldClim Version2 (Fick & Hijmans, 2017). [d]The mainstem station LW3 is located downstream the confluence of the Dasha River. [e]The sediment grain size described here is measured by sieving and weighing (Deng et al., 2019).

Palaeozoic Tailuko schist and marble along the downstream toward the Philippine Sea (Figure 1a). Slate, schist and marble account for 22%, 56%, and 22% of the total drainage area, respectively. In particular, no marble outcrops are present in the tributaries from the upper reaches (Waheir and Dasha). The areal extent of marble slightly increases along the mid-lower mainstem (Table 2). The major soil types in the Hualien County, where the Liwu Basin is located, include Entisols and Inceptisols with moderately alkaline pH (Chen et al., 2015), and the soil thickness is commonly thin at 0.2–0.9 m (Hemingway et al., 2018).

The Liwu Basin with a river length of ~58 km and an area of ~620 km^2 is characterized by steep slopes. From upstream to downstream, the basin-averaged local slope increases from 30° to 36°. Below the confluence of the Dasha River, the basin-averaged slope is uniform at 35°–36° (Table 2). Although the Liwu Basin locally bears multiple transient geomorphic features such as hanging valleys (Wobus et al., 2006), topographic steady state appears to prevail over a larger scale, as evidenced by relatively constant topographic metrics (e.g., channel steepness) in the middle part of the Central Range (Chen & Willett, 2016) including the Liwu Basin. Over decadal scales, 14 Mt of suspended load is discharged annually to the Philippine Sea despite the small basin size (Dadson et al., 2003). In particular, the vertical incision of the river channel can exceed 100 mm within two typhoon seasons (Hartshorn et al., 2002).

3. Samples and Methods

3.1. Sampling Details

We carried out a sampling campaign along the Liwu River (Figure 1) in early June 2017 prior to the typhoon season. Bedload samples were collected at three mainstem locations (downstream the Dasha confluence, at a mid-reach point, and close to the outlet) and from three tributaries (Waheir, Dasha, and Shakadang). Geomorphological characteristics of sampled basins are provided in Table 2, including a brief description of all sediment samples. At each location, two samples deposited at different positions (e.g., in the river channel vs. on the high-standing bedrock) or with visually different sediment grain-sizes (e.g., silt vs. sand) were collected in close vicinity, except the Shakadang River where only one sample was chosen. In total, 11 bedload

10.1029/2021JF006221

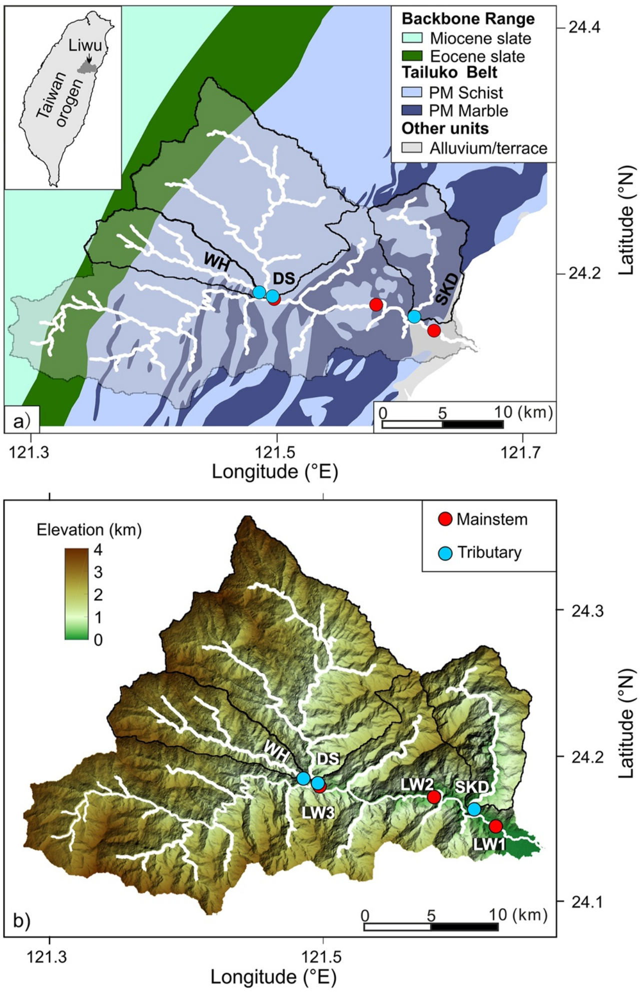

Figure 1. (a) Geological background and (b) topography of the Liwu Basin. SKD: Shakadang River; DS: Dasha River; WH: Waheir River; PM: Paleozoic-Mesozoic. The outline of sampled tributaries is delineated in black. Two samples were collected within a few meters' distance at each sampling location except at SKD (Table 2).

samples were used for chemical analysis to capture the range of natural variability in a setting affected by highly variable sediment transport.

3.2. Application of ^{10}Be(meteoric)/^{9}Be Ratios in Mixed Lithologies Including Marble

To quantify Earth surface erosion and weathering, von Blanckenburg et al. (2012) developed a steady-state mass balance framework for the ^{10}Be(meteoric)/^{9}Be system. After delivery to Earth's surface, meteoric ^{10}Be adsorbs onto mineral surfaces or co-precipitates with amorphous (called "am-ox") and crystalline (called "x-ox") Fe- and Al- oxides and hydroxides. This ^{10}Be pool exchanges with dissolved ^{10}Be through desorption-adsorption or dissolution-precipitation reactions and is thus called the "reactive" (reac) fraction. Analogously, ^{9}Be enters the weathering zone in the dissolved form by release from bedrock during weathering and is assumed to equilibrate with ^{10}Be in solution prior to reactive phase formation. Any associated isotope fractionation is smaller than analytical uncertainty and indeed minor compared to the variability in riverine ^{10}Be/^{9}Be ratios (e.g., orders of magnitudes). The resulting concentrations are called $[^{10}Be]_{reac}$ (in at/kg) and $[^{9}Be]_{reac}$ (in mg/kg), respectively. The ^{10}Be(meteoric)/^{9}Be ratio in the reactive phase is less sensitive to Be retentivity and hydraulic sorting (i.e., variations in sediment grain-size) (Wittmann et al., 2012) compared to single meteoric ^{10}Be concentrations (Singleton et al., 2016). The ^{10}Be(meteoric)/^{9}Be-derived denudation rate (D_{met}, in kg/m²/yr) is thus calculated as:

$$D_{met} = \frac{F_{met}^{10Be}}{\left(\frac{^{10}Be}{^{9}Be}\right)_{reac} \times \left[^{9}Be\right]_{parent}} \times \left(\frac{\left[^{9}Be\right]_{min}}{\left[^{9}Be\right]_{reac}} + 1\right) \tag{1}$$

where F_{met}^{10Be} (in at/m²/yr) is the depositional flux of ^{10}Be, $[^{9}Be]_{parent}$ (mg/kg) is the ^{9}Be present in the parent bedrock prior to weathering, and the silicate residual "min" phase that hosts the immobile remainder of ^{9}Be is termed $[^{9}Be]_{min}$ (mg/kg). The unit of D_{met} can be converted to mm/yr using a density of 2.65×10^3 kg/m³. This equation is derived from a steady-state framework based on the assumptions that isotopic ratios of all the eroded sources are well-mixed, and that all atmospheric ^{10}Be input into the catchment is exported by riverine transport at the same rate. We will evaluate the validity of these assumptions in the landslide-dominated Liwu River in Section 5.4. The amount of ^{9}Be mobilized during weathering, termed f_{reac}, is the ratio of $[^{9}Be]_{reac}$ to the sum of $[^{9}Be]_{min}$ and $[^{9}Be]_{reac}$:

$$f_{reac} = \frac{\left[^{9}Be\right]_{reac}}{\left[^{9}Be\right]_{reac} + \left[^{9}Be\right]_{min}} \tag{2}$$

The detailed derivation for Equations 1 and 2 is given in von Blanckenburg et al. (2012). The two equations are simplified from those that also account for the dissolved fluxes of Be isotopes ($[^{9}Be]_{diss}$, in mg/l and $[^{10}Be]_{diss}$, in atoms/l). In the Liwu River we consider that the dissolved Be fluxes are minor as justified later in this section. In general, the successful application of the new proxy relies on four requirements (1–4) repeated below (von Blanckenburg et al., 2012), and in the Liwu River draining mixed lithologies including marble, also requires additional lithology-specific information (5):

(1) The atmospheric depositional flux F_{met}^{10Be} must be known. The knowledge of F_{met}^{10Be} is a prerequisite for any meteoric ^{10}Be application. Previous studies on the Taiwan orogen estimated ^{10}Be depositional flux by e.g., assuming a constant rain ^{10}Be concentration determined from other regions (Tsai et al., 2008;

10.1029/2021JF006221

You et al., 1988). Here we use an up-to-date, site-specific flux of $0.77 \pm 0.11 \times 10^6$ at/cm^2/yr constrained by meteoric ^{10}Be profiles of Holocene river terraces in Taiwan (Deng et al., 2021). Other approaches for determination of ^{10}Be depositional fluxes, including general circulation models (GCMs) (Heikkilä & von Blanckenburg, 2015) and rainfall ^{10}Be-based fitting equation (Graly et al., 2011), are commonly applied over larger spatial scales and may overestimate ^{10}Be fluxes in our study area (Deng et al., 2021; Deng, Wittmann, & von Blanckenburg, 2020).

(2) The concentration of ^9Be contained in unweathered bedrock ($[^9Be]_{parent}$) needs to be known. $[^9Be]_{parent}$ in small catchments can be constrained by two strategies, which are (a) area-weighing of rock ^9Be concentrations from each geological unit or (b) linear regression between concentrations of an immobile element (e.g., Al) and Be in bedrock combined with determining a representative concentration of that immobile element in river sediment (Dannhaus et al., 2018). Note, however, that where variability of rock ^9Be concentration is large, as observed in the Liwu basin (Figure 1a and Table S1 in Supporting Information S1), the area-weighing strategy could deliver biased results, because it assumes that ^9Be contributions of all lithologies are proportional to their outcrop area (rather than sediment contribution). The linear regression approach, in contrast, requires that Be and an immobile element in rocks are enriched in similar mineral types; and further that mixing of this immobile element in river sediment eroded from source rocks is indicative of mixing of source rock ^9Be. We thus adopt the linear regression approach here (see details in Section 5.2.2).

(3) A representative f_{reac} can be estimated from the $[^9Be]_{min}/[^9Be]_{reac}$ ratio in river sediment. Even though the ratio of $[^9Be]_{min}$ to $[^9Be]_{reac}$ in Equation 2 can eliminate the dilution effect of quartz (lack of Be and higher abundance in coarser-grained sediment), this ratio may be biased by sorting as $[^9Be]_{reac}$ is potentially enriched over $[^9Be]_{min}$ in fine sediments of higher adsorption capability (von Blanckenburg et al., 2012; Wittmann et al., 2012). In the Liwu River, the suspended sediment fraction is estimated to dominate the total sediment load based on an empirical estimation on the fraction of suspended load (Turowski et al., 2010). Hence, to minimize the grain-size bias, sieving to a narrow grain-size fraction of bedload that is similar to the grain-size range of suspended load will likely provide $[^9Be]_{min}/[^9Be]_{reac}$ of the bulk sediment load.

(4) The partitioning of Be flux into the dissolved pool must be estimated. The existence of a large pool of total dissolved Be (operationally defined, entailing the sum of truly dissolved Be and colloidal Be), if not included for calculation, can lead to overestimation of denudation rates. Although $(^{10}Be/^9Be)_{reac}$ in Equation 1 is not affected by this loss, a bias might arise if the $[^9Be]_{min}/[^9Be]_{reac}$ increases by partitioning of reactive ^9Be into the total dissolved pool. However, this bias can be quantified (von Blanckenburg et al., 2012) as the fraction of total dissolved flux of Be isotopes in riverine export can be estimated using the pH-dependent Be partition coefficient K_d (calculated from the ratio of $[Be]_{reac}$ to $[Be]_{diss}$, in l/kg). When K_d is much higher than the ratio of runoff (q, in m/yr) to erosion rate (E, in kg/m^2/yr), the loss of reactive Be into the total dissolved flux is negligible (von Blanckenburg et al., 2012). Specifically, the bias (%) on denudation rate estimates arising from Be retentivity issues can be quantified as (von Blanckenburg et al., 2012):

$$\text{Bias}\left(\%\right) = \frac{q}{E \times K_d} \times f_{\min} \times 100 \tag{3}$$

The basin-averaged q/E derived from decadal gauging data (Dadson et al., 2003) reaches ∼73 l/kg. In comparison, a pH of >7 prevails along the dissolved pathways (soil interflow, groundwater and surface runoff) in the Liwu River (Calmels et al., 2011), corresponding to a minimum K_d value of $\sim 1.7 \times 10^5$ l/kg based on empirically derived K_d-pH relationships (Brown et al., 1992; You et al., 1989). When using a $f_{\min}$ (the proportion of $[^9Be]_{min}$ in bulk ^9Be) of ∼0.9 (an average value of all Liwu samples), the resulting bias% on denudation rate is <1% for not including the dissolved Be pool. Hence, we argue that the partitioning of Be into the total dissolved fraction and the potential overestimation of denudation rate are minor here.

(5) Components of Be isotopes associated with carbonate minerals can be distinguished from other hydroxide-bound reactive Be by specific extractions. Sediment sampled from river basins in which abundant carbonate rocks exist likely contains different components of Be associated with two kinds of carbonate fractions: (a) detrital carbonate that has not exchanged with the ^{10}Be pool since its formation in Palaeozoic times (in the Liwu case), containing no ^{10}Be (that has decayed) and some ^9Be (as part of $[^9Be]_{min}$); (b) secondary carbonate that has likely equilibrated with the dissolved Be pool in soil

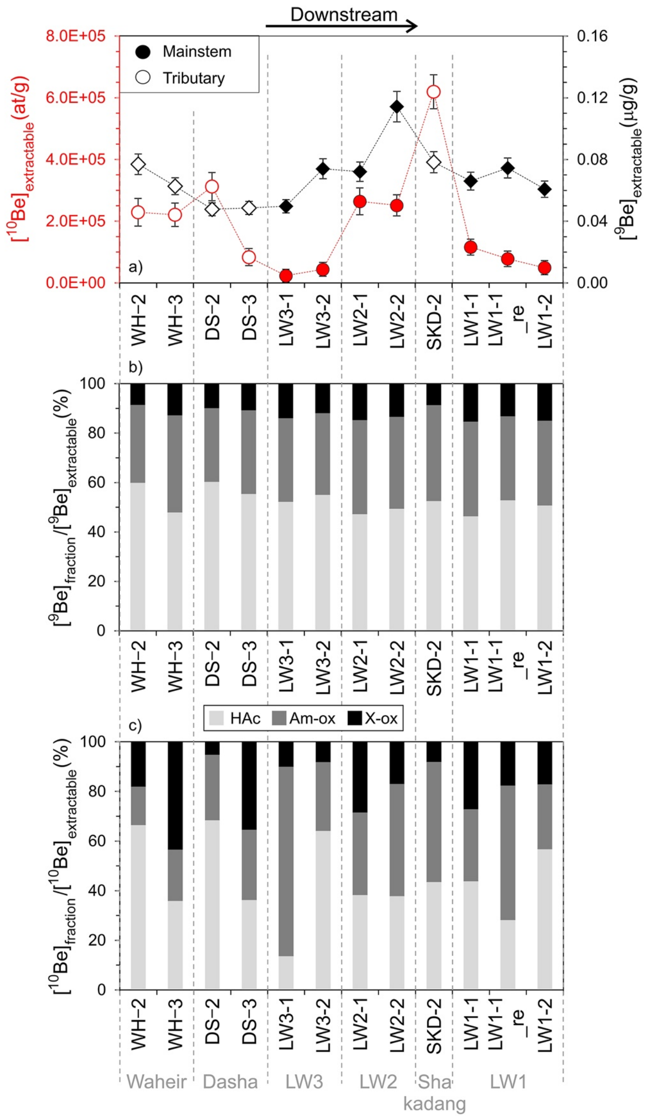

Figure 2. (a) Total chemically extractable ^{10}Be and ^{9}Be concentrations ($[^{10}Be]_{extractable}$ and $[^{9}Be]_{extractable}$, sum of HAc, am-ox, and x-ox fractions) in Liwu River sediments. (b and c) show the concentration of ^{9}Be and ^{10}Be in each fraction normalized to the total extractable concentration. WH-2 and -3, DS-2 and -3, LW3-1 and -2, LW2-1 and -2, and LW1-1 and -2 were collected at the same location. LW1-1_re is a lab replicate for LW1-1.

solutions during its precipitation, which must be regarded as part of the reactive Be pool ($[^{10}Be]_{reac}$ and $[^{9}Be]_{reac}$) for D_{met} calculation. Hence, we added an additional extraction step to our original method (Wittmann et al., 2012): using acetic acid prior to the extraction of amorphous and crystalline oxides. This acetic acid step will mobilize different forms of Be associated with (both primary and secondary) carbonate minerals and a potentially adsorbed pool that is released in acidic environments (You et al., 1989).

3.3. Analytical Methods

River sediment samples taken from the field were first subsampled by the coning-quartering method, and then dry-sieved to a narrow grain-size range of 30–63 μm according to requirement three (Section 3.2). After overnight oven-drying, the extraction of ^{10}Be and ^{9}Be was performed according to Wittmann et al. (2012), with an amendment for carbonate-rich sediments. About 1 g of the sieved sediment was first treated with 8 ml 1 M acetic acid at 70°C with mild shaking for 12 hr (called HAc fraction), a procedure that aims to mobilize the carbonate fraction (adapted from Hohl et al., 2015). We monitored solution-pH and a value of lower than 5 was maintained to ensure the dissolution of carbonate minerals. The post-HAc leach residue was dried and weighed again to determine the mass fraction of carbonate removed during this step. Subsequently, the residue was treated according to the original extraction method (Wittmann et al., 2012) with 15 ml 0.5 M HCl and mild shaking at room temperature for 24 h to extract the amorphous hydroxides (called am-ox fraction). The residue was then treated with 15 ml 1 M $NH_2OH\cdot HCl$ at 80°C with manual shaking every 10 min for 4 hr to extract crystalline hydroxides (called x-ox fraction). The post-(am-ox + x-ox) leach residue was dried again and weighed. All chemically extracted fractions and the remaining solid residue (called min fraction) were treated with HF and aqua regia mixtures to fully decompose the sample matrix.

Once fully dissolved in 3 M HNO_3, all chemically extractable fractions (HAc, am-ox, x-ox) were split into two aliquots. One split and the min fraction were analyzed for stable ^{9}Be and major elemental concentrations by Inductively Coupled Plasma-Optical Emission Spectroscopy (ICP-OES, Varian 720-ES) at GFZ Potsdam. The second split of extractable fractions was spiked with ^{9}Be carrier of known weight (~110 μg Be) and purified for ^{10}Be analysis according to established methods (e.g., von Blanckenburg et al., 1996). ^{10}Be concentrations were obtained from accelerator mass spectrometry (AMS) measurements of $^{10}Be/^{9}Be$ ratios (with carrier) at University of Cologne, relative to the standard KN01-6-2 with a $^{10}Be/^{9}Be$ ratio of 5.35×10^{-13} (Dewald et al., 2013) that is consistent with the ^{10}Be half-life of 1.39 Myr (Chmeleff et al., 2010). We used a blank $^{10}Be/^{9}Be$ ratio of $1.4 \pm 0.6 \times 10^{-15}$ ($n = 6$) for blank correction of ^{10}Be concentrations.

4. Results

Concentrations of ^{10}Be and ^{9}Be in different chemical fractions are shown in Figure 2 and Table 3.

The chemical extractable ^{9}Be concentration contained in the summed HAc, am-ox and x-ox fractions is low and uniform, showing little variation between 0.05 and 0.08 μg/g (Figure 2a) for most samples except LW2-2 (mainstem Liwu), where the extractable ^{9}Be concentration is slightly higher (0.11 μg/g). Mainstem and tributary samples show no clear difference in ^{9}Be concentrations. In contrast, the ^{10}Be concentration in the

Table 3
Concentrations of Meteoric ^{10}Be and Stable ^{9}Be

Sample ID	Carbonate contribution[a] (wt%)	$[^{10}Be]_{HAc}$ [b,c] ($\times 10^5$ atoms/g)	$[^{10}Be]_{am\text{-}ox}$ [b,c] ($\times 10^5$ atoms/g)	$[^{10}Be]_{x\text{-}ox}$ [b,c] ($\times 10^5$ atoms/g)	$[^{9}Be]_{HAc}$ [b,c] (μg/g)	$[^{9}Be]_{am\text{-}ox}$ [b,c] (μg/g)	$[^{9}Be]_{x\text{-}ox}$ [b,c] (μg/g)	$[^{9}Be]_{min}$ [b,c] (μg/g)
WH-2	7.5	1.52 ± 0.38	0.35 ± 0.15	0.41 ± 0.19	0.046 ± 0.002	0.024 ± 0.001	0.007 ± 0.0003	0.56 ± 0.03
WH-3	7.8	0.79 ± 0.27	0.46 ± 0.18	0.96 ± 0.20	0.030 ± 0.002	0.025 ± 0.001	0.008 ± 0.0004	0.58 ± 0.03
DS-2	6.7	2.14 ± 0.40	0.82 ± 0.19	0.17 ± 0.13	0.029 ± 0.001	0.014 ± 0.001	0.005 ± 0.0002	0.37 ± 0.02
DS-3	6.7	0.30 ± 0.17	0.24 ± 0.16	0.30 ± 0.14	0.027 ± 0.001	0.016 ± 0.001	0.005 ± 0.0003	0.49 ± 0.02
LW3-1	5.1	0.03 ± 0.13	0.18 ± 0.12	0.02 ± 0.11	0.026 ± 0.001	0.017 ± 0.001	0.007 ± 0.0003	0.50 ± 0.03
LW3-2	5.2	0.28 ± 0.15	0.12 ± 0.13	0.04 ± 0.11	0.041 ± 0.002	0.024 ± 0.001	0.009 ± 0.0004	0.92 ± 0.05
LW2-1	7.3	1.01 ± 0.28	0.88 ± 0.21	0.75 ± 0.26	0.034 ± 0.002	0.027 ± 0.001	0.011 ± 0.0005	0.71 ± 0.04
LW2-2	5.3	0.95 ± 0.20	1.14 ± 0.23	0.43 ± 0.16	0.056 ± 0.003	0.043 ± 0.002	0.015 ± 0.0008	1.16 ± 0.06
SKD-2	16.3	2.69 ± 0.35	3.00 ± 0.37	0.50 ± 0.20	0.041 ± 0.002	0.030 ± 0.002	0.007 ± 0.0003	1.07 ± 0.05
LW1-1	5.8	0.51 ± 0.18	0.34 ± 0.12	0.32 ± 0.14	0.031 ± 0.002	0.025 ± 0.001	0.010 ± 0.0005	0.91 ± 0.05
LW1-1_re[d]	4.9	0.22 ± 0.15	0.42 ± 0.15	0.14 ± 0.13	0.039 ± 0.002	0.025 ± 0.001	0.010 ± 0.0005	0.93 ± 0.05
LW1-2	7.0	0.28 ± 0.14	0.13 ± 0.13	0.08 ± 0.12	0.031 ± 0.002	0.021 ± 0.001	0.009 ± 0.0005	0.70 ± 0.03

[a]For estimation of the mass fraction removed by the HAc step, the residue was dried and weighed after the acetic acid leach. The calculated weight percentage (carbonate contribution, wt%) is derived from the carbonate mass relative to the initial solid sample mass. [b]Measured chemical fractions comprise fraction associated with carbonate minerals (HAc), amorphous oxide-bound fraction (am-ox), crystalline oxide-bound fraction (x-ox), and silicate residual fraction (min). All concentrations are calculated relative to the initial solid sample mass (~1 g). [c]All uncertainties denote 1σ analytical errors. For ^{9}Be measurements using ICP-OES, the given uncertainty (5%) is the long-term repeatability which is propagated into ^{10}Be/^{9}Be ratios. For ^{10}Be measurements, the analytical uncertainty from AMS is propagated into ^{10}Be/^{9}Be ratios. We use a blank ^{10}Be/^{9}Be ratio of $1.4 \pm 0.6 \times 10^{-15}$ ($n = 6$), corresponding to approximately $1.0 \pm 0.5 \times 10^4$ atoms of ^{10}Be added by carrier, for blank correction of ^{10}Be concentrations. [d]LW1-1_re is a laboratory replicate of LW1-1, obtained from a split of the same sample prior to initial weighing. Although the difference in [^{10}Be] of each fraction between lab replicates is large due to low concentrations, they generally agree within uncertainty.

chemical extractable fraction shows a larger, ca. 30-fold variability, ranging from 0.23×10^5 to 6.19×10^5 atoms/g (Figure 2a). In the mainstem, samples at location LW3 (close to the Liwu upstream) and at location LW1 (near the river mouth) show extremely low concentrations (0.23–1.16 $\times 10^5$ atoms/g), whereas in the middle reach at LW2, a higher ^{10}Be concentration (2.58×10^5 atoms/g on average) is observed. For the tributaries, the ^{10}Be concentration in the chemical extractable fraction distinctly differs between both samples from the Dasha River (0.84×10^5 vs. 3.12×10^5 atoms/g), whereas both Waheir samples (WH) are consistent with an average value of 2.25×10^5 atoms/g. The Shakadang sediment sample (SKD-2) shows the highest chemical extractable ^{10}Be concentration of 6.19×10^5 atoms/g amongst all samples.

The partitioning between the three extractable fractions (each fraction normalized to the sum of HAc, am-ox and x-ox fractions) differs between ^{10}Be and ^{9}Be (Figures 2b and 2c). ^{9}Be percentages in each of these chemical fractions are generally uniform for all samples, with 52.5 ± 4.6% (±standard deviation) contained in the HAc fraction, 35.2 ± 3.1% in the am-ox fraction, and 12.4 ± 2.4% in the x-ox fraction, respectively. In contrast, the variation in ^{10}Be percentage between the extractable fractions is larger. The ^{10}Be percentage in the HAc fraction is 44.4 ± 16.6%, 35.9 ± 17.1% in the am-ox fraction and 19.7 ± 11.8% in the x-ox fraction, respectively.

^{10}Be(meteoric)/^{9}Be ratios vary over two orders of magnitude in all these fractions, from 1.83×10^{-12} to 1.11×10^{-10} in the HAc fraction, from 7.46×10^{-12} to 1.48×10^{-10} in the am-ox fraction, and in the x-ox fraction from 5.08×10^{-12} to 1.79×10^{-10} (Figure 3). Because of fast erosion and thus $[^{10}Be]_{sample}$ being similar to $[^{10}Be]_{blank}$, blank-corrected ^{10}Be(meteoric)/^{9}Be ratios of total extractable fraction in LW3-1, LW3-2 and LW1-2 (Table 4) show high relative analytical error (>40%) that can explain the discrepancy between samples at each station. For each sample ^{10}Be(meteoric)/^{9}Be ratios of the three chemical fractions mostly agree within uncertainties, shown by (a) the ratio of relative standard deviation among the three fractions to their average relative analytical error (Table S3 in Supporting Information S1), which mostly varies around 1 (0.96 on average), except WH-3 that has a ratio of 3.2, and (b) the consistency in distribution of ^{10}Be(meteoric)/^{9}Be ratios in all the samples between the three fractions from one-way analysis of variance test ($p = 0.27$). This

10.1029/2021JF006221

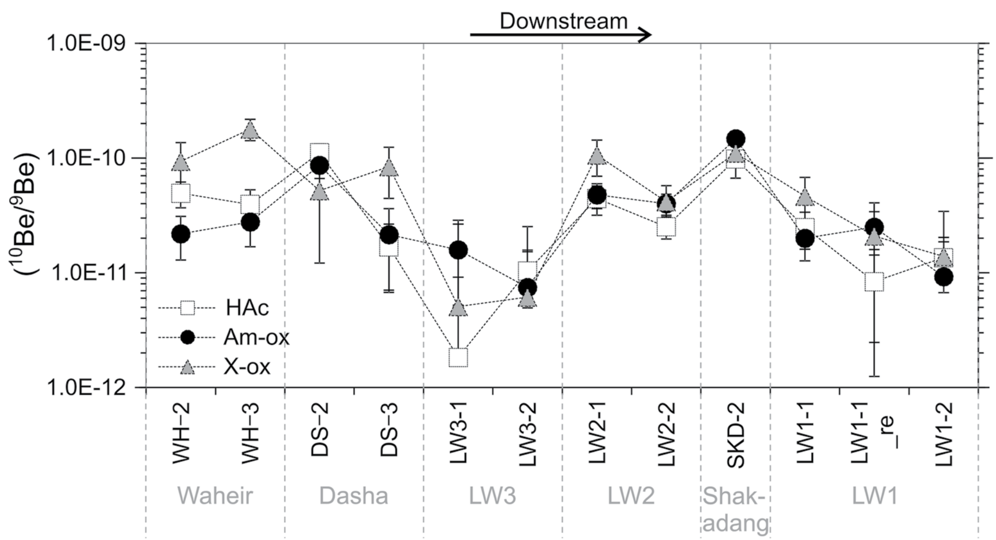

Figure 3. ^{10}Be(meteoric)/^{9}Be ratios of HAc, am-ox, and x-ox fractions. The relative analytical uncertainty of some samples can be large (e.g., >50%) due to low ^{10}Be concentrations that are similar to the blank ^{10}Be level, hinting at extremely fast erosion. Distribution of ^{10}Be(meteoric)/^{9}Be ratios in all the samples is indistinguishable between the three fractions based on one-way analysis of variance test ($p = 0.27$).

agreement in ^{10}Be(meteoric)/^{9}Be ratios between fractions suggests that the Be incorporated into the three fractions stems from the same dissolved pool. Overall, tributary samples show a higher total extractable ^{10}Be(meteoric)/^{9}Be ratio than the mainstem samples ($p < 0.05$ from a two-sided Wilcoxon rank sum test).

Table 4
^{10}Be(meteoric)/^{9}Be Ratios, Be-Specific Weathering Intensity ($f_{reac\text{-}c}$), $[^{9}Be]_{parent}$ and Denudation Rates Derived From Blank-Corrected $(^{10}Be/^{9}Be)_{reac\text{-}c}$ (D_{met}) and Blank-Uncorrected Ratios ($D_{met\text{-}noblkcorr}$)

Sample ID	$(^{10}Be/^{9}Be)_{HAc}$ ($\times10^{-11}$)	$(^{10}Be/^{9}Be)_{am\text{-}ox}$ ($\times10^{-11}$)	$(^{10}Be/^{9}Be)_{x\text{-}ox}$ ($\times10^{-11}$)	$(^{10}Be/^{9}Be)_{reac\text{-}c}$ ($\times10^{-11}$)	$f_{reac\text{-}c}$ [a]	$[^{9}Be]_{parent}$ [b] (μg/g)	D_{met} [a,c] (mm/yr)	$D_{met\text{-}noblkcorr}$ [c] (mm/yr)
WH-2	4.93 ± 1.25	2.19 ± 0.90	9.33 ± 4.32	4.45 ± 0.88	0.121 ± 0.008	1.01 ± 0.07	8.0 ± 2.1	
WH-3	3.94 ± 1.35	2.77 ± 1.09	17.94 ± 3.78	5.27 ± 0.92	0.097 ± 0.007	1.02 ± 0.07	8.3 ± 2.0	
DS-2	11.11 ± 2.14	8.64 ± 2.02	5.21 ± 3.99	9.79 ± 1.47	0.114 ± 0.008	0.71 ± 0.05	5.5 ± 1.3	
DS-3	1.68 ± 0.98	2.15 ± 1.48	8.42 ± 3.98	2.57 ± 0.85	0.091 ± 0.006	0.87 ± 0.06	21.5 ± 8.0	
LW3-1	0.18 ± 0.73	1.59 ± 1.06	0.51 ± 2.36	0.70 ± 0.62	0.090 ± 0.006	0.72 ± 0.05	*95.4 ± 85.7*	>30 ± 8
LW3-2	1.04 ± 0.54	0.75 ± 0.78	0.61 ± 1.91	0.89 ± 0.45	0.074 ± 0.005	1.34 ± 0.09	*49.1 ± 26.4*	>23 ± 6
LW2-1	4.44 ± 1.26	4.79 ± 1.17	10.62 ± 3.69	5.49 ± 0.93	0.093 ± 0.006	1.06 ± 0.07	8.1 ± 1.9	
LW2-2	2.51 ± 0.55	4.00 ± 0.83	4.17 ± 1.56	3.29 ± 0.46	0.090 ± 0.006	1.63 ± 0.11	9.0 ± 2.0	
SKD-2	9.80 ± 1.38	14.77 ± 1.97	11.04 ± 4.39	11.80 ± 1.12	0.068 ± 0.005	1.58 ± 0.10	3.4 ± 0.7	
LW1-1	2.48 ± 0.88	2.00 ± 0.73	4.64 ± 2.13	2.63 ± 0.59	0.068 ± 0.005	1.27 ± 0.08	19.2 ± 5.4	
LW1-1_re	0.84 ± 0.59	2.50 ± 0.90	2.10 ± 1.97	1.57 ± 0.51	0.074 ± 0.005	1.31 ± 0.09	28.5 ± 10.5	
LW1-2	1.36 ± 0.68	0.92 ± 0.94	1.39 ± 2.04	1.21 ± 0.56	0.080 ± 0.005	1.02 ± 0.07	*43.7 ± 21.6*	>22 ± 5

[a]In the Liwu case, we define the "reactive" pool that exchanges with the dissolved pool as the sum of all the chemical extractable fractions (termed reac-c), which include HAc, am-ox and x-ox fractions (see Section 5.1). The reac-c fraction is used to calculate $f_{reac\text{-}c}$ (Equation 2, using $[^{9}Be]_{reac\text{-}c}$ from Table 3) and D_{met} (Equation 1, using $(^{10}Be/^{9}Be)_{reac\text{-}c}$) given here. [b]Values are obtained from a linear fitting equation between Al and Be concentrations measured in Taiwan rock samples ($n = 21$) following Dannhaus et al. (2018) (see Section 5.2.2 for details). Area-weighted bedrock ^{9}Be concentration for each sampled upstream basin is provided in Table S2 in Supporting Information S1 for comparison. [c]Due to the large uncertainty propagated from blank-corrected $(^{10}Be/^{9}Be)_{reac\text{-}c}$, uncertainty in D_{met} of LW1-2 and LW3-1, -2 (in italic) are quite high. A lower-limit first-order estimate of denudation, termed $D_{met\text{-}noblkcorr}$, is thus derived from blank-uncorrected $(^{10}Be/^{9}Be)_{reac\text{-}c}$ (i.e., the ^{10}Be derived from the ^{9}Be carrier was not subtracted for calculating $[^{10}Be]_{reac\text{-}c}$). The given uncertainty thus does not include that of blank ^{10}Be/^{9}Be. Such estimate yields an upper-limit $(^{10}Be/^{9}Be)_{reac\text{-}c}$ and thus a minimum denudation rate.

^{10}Be and ^{9}Be concentrations, ^{10}Be(meteoric)/^{9}Be ratios, and major elemental data are provided in Tables 3 and 4 and Table S4 in Supporting Information S1, respectively.

5. Discussion

5.1. Partitioning of Be Into the HAc Fraction and Definition of the Reactive Fraction in the Liwu River

To define the reactive fraction in the Liwu River that should be in equilibrium with the dissolved fraction, we investigate the way in which Be is hosted by the HAc fraction. Specifically, we explore Be associated with (a) primary or (b) secondary carbonate minerals, or (c) Be that was sorbed to particle surfaces. For cases (b and c) the HAc fraction should be included in the operationally defined reac fraction, as these two reservoirs comprise Be equilibrated with the dissolved Be fraction. We adopted two approaches to discriminate between these options.

First we inspect ^{10}Be(meteoric)/^{9}Be ratios found in the extractions. If primary carbonate were the dominant source of $[\mathrm{Be}]_{\mathrm{HAc}}$, $(^{10}\mathrm{Be}/^{9}\mathrm{Be})_{\mathrm{HAc}}$ would be expected to be much lower compared to those in am-ox and x-ox fractions, because all ^{10}Be once associated with primary carbonate of Paleozoic-Mesozoic ages (Figure 1) should have decayed. However, the general agreement (within uncertainties) between ^{10}Be(meteoric)/^{9}Be ratios in the three chemical fractions (HAc, am-ox and x-ox) for the majority of samples (Figure 3) suggests if anything an only minor contribution of primary carbonate to $[\mathrm{Be}]_{\mathrm{HAc}}$.

Second, we predict the expected primary carbonate contribution to $[\mathrm{Be}]_{\mathrm{HAc}}$ using $[\mathrm{Be}]_{\mathrm{marble}}$. To this end we first estimated the fraction of the mass removed from the initial solid sample during the acetic acid leaching step which comprises 4.9%–16.3% of the bulk weight for all samples (Table 3). Second, we used the ^{9}Be concentration in bedrock marble (0.028 ± 0.001 μg/g, Table S1 in Supporting Information S1) collected from two different locations to estimate the maximum contribution of ^{9}Be to the HAc fraction that is associated with primary carbonate minerals. Using a carbonate contribution of 16.3 wt% (SKD-2 draining mainly marble) as an upper limit, a ^{9}Be concentration of only 0.005 μg/g is predicted in bulk sediment. This ^{9}Be concentration is much lower than $[^{9}\mathrm{Be}]_{\mathrm{HAc}}$ of 0.041 μg/g measured in SKD-2 (Table 3), showing that primary carbonate minerals in this case cannot be the dominating reservoir for $[^{9}\mathrm{Be}]_{\mathrm{HAc}}$.

Given the evidence provided, we propose that Be isotopes contained in the HAc fraction are dominated by different components associated with secondary carbonate and/or adsorption that can be extracted in the acetic acid step. We thus define the reactive fraction in the Liwu case as the sum of all the chemical extractable fractions, that are HAc, am-ox and x-ox fractions, termed as $[^{10}\mathrm{Be}]_{\text{reac-c}}$ (in atoms/kg) and $[^{9}\mathrm{Be}]_{\text{reac-c}}$ (in mg/kg). Corresponding ^{10}Be/^{9}Be ratios are termed as $(^{10}\mathrm{Be}/^{9}\mathrm{Be})_{\text{reac-c}}$. We apply this modified framework to Equations 1 and 2.

5.2. Be-Specific Weathering Intensity and $[^{9}\mathrm{Be}]_{\mathrm{parent}}$ Determination

5.2.1. Weathering Intensity ($f_{\text{reac-c}}$)

We calculate the fraction of Be released during weathering of Be-bearing primary minerals and partitioned into reactive fractions using Equation 2 and the reac-c fraction ($[^{9}\mathrm{Be}]_{\text{reac-c}}$). The $f_{\text{reac-c}}$ can be seen as a Be-specific "weathering intensity," expressed as fraction of reactive ^{9}Be relative to bulk Be concentration. Its estimate relies on the assumption that the contribution of Be from primary carbonate minerals to $[^{9}\mathrm{Be}]_{\text{reac-c}}$ is minor as justified in Section 5.1. $f_{\text{reac-c}}$ is 0.09–0.12 in the slowly eroding (i.e., high ^{10}Be/^{9}Be ratios) tributaries (Waheir and Dasha) and slightly lower at 0.07–0.09 in the rapidly eroding (i.e., low ^{10}Be/^{9}Be ratios) mainstem. We compare these values to those from global large river basins of similar sedimentary lithology where f_{reac} data exist. f_{reac} in the Amazon basin vary from 0.09 to 0.55 with an average value of 0.30 ($n = 37$) (Wittmann et al., 2015), the range of f_{reac} in the Ganga basin is between 0.10 and 0.57 with an average value of 0.29 ($n = 20$) (Rahaman et al., 2017), and a global average value of 0.20 ± 0.08 (standard deviation) for f_{reac} is suggested by von Blanckenburg and Bouchez (2014). A lower $f_{\text{reac-c}}$ in the Liwu Basin is compatible with the decrease of weathering intensity in fast-eroding settings (Dixon & von Blanckenburg, 2012).

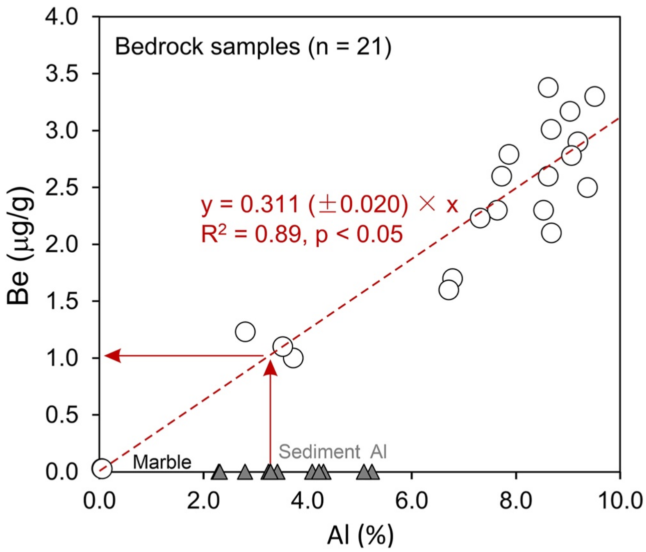

Figure 4. Determination of $[^9Be]_{parent}$ from concentrations of Al ($[Al]_{rock}$) and Be ($[Be]_{rock}$) measured in bedrock around our study area (n = 21, open circles) using a linear regression approach following Dannhaus et al. (2018). The resulting linear-fitting equation is used to constrain $[^9Be]_{parent}$ for each sampled sub-catchment. Al concentrations measured from sediment samples (triangles) are plotted on the X-axis for comparison. Red arrows shown exemplify how a $[^9Be]_{parent}$ was derived: for LW1-2, the [Al] of 3.29% measured in sediment (sum of [Al] in HAc, am-ox, x-ox and min fractions, Table S4 in Supporting Information S1) corresponds to a $[^9Be]_{parent}$ of 1.02 ± 0.07 µg/g in bedrock.

5.2.2. Determination of $[^9Be]_{parent}$

To constrain $[^9Be]_{parent}$ based on measurements of local bedrock samples around the Liwu Basin (n = 21, Table S1 in Supporting Information S1), we use a linear-fitting approach between concentrations of an immobile element (Al in this case) and Be in bedrock samples following Dannhaus et al. (2018). Be is enriched in silicate minerals similar to Al, and Be commonly substitutes into silicate minerals for Al^{3+} by pairing with other ions (Ryan, 2002). As such, the similarity in mineralogical host between both elements suggests their similar behaviors during sediment mixing from different source rocks. However, Be can be subject to weathering or precipitation processes and thus the source rock Be $[^9Be]_{parent}$ can be modified during sediment transport, while Al as an immobile element is expected to behave more conservatively especially under conditions of low weathering intensity (Garzanti & Resentini, 2016) and a narrow grain-size range. Hence, by substituting [Al] of each sediment sample into this linear-fitting equation (Figure 4) we can derive a corresponding $[^9Be]_{parent}$.

In compiled rock samples including marble (n = 21), we find Al and Be to be well-correlated (R^2 = 0.89, $p < 0.05$, Figure 4), whereas the correlation coefficients between other major immobile elements (Fe, K, and Ti) and Be, respectively, are lower (0.66–0.78, Table S1 in Supporting Information S1). The resulting fitting equation is $[Be]_{rock} = 0.311 \times [Al]_{rock}$ ([Be] in µg/g and [Al] in %), with an uncertainty of the coefficient of $[Al]_{rock}$ of 0.020 (95% confidence) that is propagated into the calculation of $[Be]_{parent}$ and D_{met}. By combining this equation and sediment Al concentrations (sum of [Al] in HAc, am-ox, x-ox and min fractions, Table S4 in Supporting Information S1), we derive $[^9Be]_{parent}$ representative for each sampled sub-catchment, ranging from 0.71 to 1.63 µg/g (Table 4). Note that even though other immobile elements show weaker correlations with Be, choosing another element for the linear regression method does not significantly change resulting $[^9Be]_{parent}$. For example, when replacing Al with K the resulting range of $[^9Be]_{parent}$ (0.87–1.70 µg/g) is similar (p = 0.33 from rank-sum test).

5.3. Denudation Rates From ^{10}Be(meteoric)/^{9}Be Ratios and Comparison With Other Approaches

Denudation rates from ^{10}Be(meteoric)/^{9}Be ratios (D_{met}) are calculated using Equation 1 and the reac-c fraction ($(^{10}Be/^9Be)_{reac\text{-}c}$ from Table 4) and shown in Figure 5. Notably, for samples with extremely low $(^{10}Be/^9Be)_{reac\text{-}c}$ and high relative standard deviation of D_{met}, we present denudation rates derived from blank-corrected ^{10}Be (D_{met}) and from ^{10}Be with no blank correction ($D_{met\text{-}noblkcorr}$) in Table 4. $(^{10}Be/^9Be)_{reac\text{-}c}$ calculated from the latter only represents an upper-limit estimate and thus $D_{met\text{-}noblkcorr}$ is a minimum estimate that can only be seen as a first-order approximation of the real denudation rate.

In the Liwu mainstem, D_{met} are highest (>30 mm/yr) close to the upstream (LW3), then decrease to 8.1–9.0 mm/yr at LW2, and finally increase again to 23.9 mm/yr near the river mouth (mean of LW1-1 and LW1-1_re). The Waheir, Dasha, and Shakadang tributaries erode at rates of 3.4–21.5 mm/yr. Note that even though D_{met} obtained for LW3 and LW1-2 is a minimum estimate, we are confident that these rates are meaningful, because the minimum rate of LW3 is similar to DS-3 measured for the large Dasha tributary close by, and LW1-2 agrees well with other samples measured at the same station. In general, two samples collected at each location agree in D_{met} within (notably large) uncertainties.

^{10}Be(meteoric)/^{9}Be-derived denudation rates in the Liwu mainstem (8.1 to >30 mm/yr) are among the highest ever reported from cosmogenic nuclides, which typically do not exceed 10 mm/yr even in tectonically active regions such as Tibetan Plateau or west Taiwan (Cook et al., 2018; Deng, Yang, et al., 2020; Derrieux et al., 2014; Scherler et al., 2014). To probe into the causes for this upper limit of denudation rate

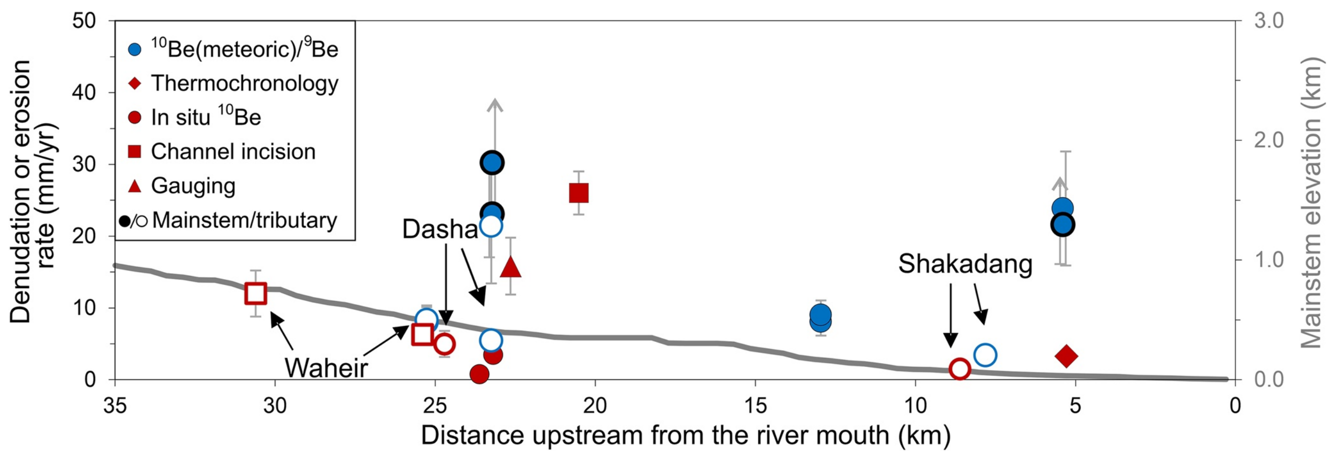

Figure 5. Spatial distribution of ^{10}Be(meteoric)/^{9}Be-derived denudation rates and other published denudation estimates in the Liwu Basin. Open symbols for each method represent tributary data. If error bars are overlapping, they are slightly shifted laterally. Symbols with thick black outlines (LW1-2 and LW3-1, -2) are calculated using $(^{10}Be/^{9}Be)_{reac\text{-}c}$ with no blank correction (i.e., $D_{met\text{-}noblkcorr}$, Table 4) and thus represent minimum estimates. Elevation swath profile along the sampled reaches of the Liwu mainstem is shown on right axis. Data sources: low-temperature thermochronology (Fellin et al., 2017), *in situ* ^{10}Be data (Derrieux et al., 2014), channel incision (Dadson et al., 2003; Schaller et al., 2005), and sediment gauging (Dadson et al., 2003). Regarding the gauging-derived suspended sediment yield we added a bedload estimate, that is, 21% of total sediment load, using an empirical relationship between drainage area (A = 435 km^2) and the fraction of suspended load (F_{sus}, %, =0.55 + 0.04 × ln(A)) (Turowski et al., 2010). A total modern sediment yield of 15.8 mm/yr hence results.

measurement from cosmogenic ^{10}Be in the Liwu River, we first need to evaluate if there is any methodological bias in such a dynamic sediment routing system.

The application of the ^{10}Be(meteoric)/^{9}Be method in the Liwu Basin can be potentially biased if there is a disequilibrium of Be isotopes between each reactive fraction and dissolved phase caused by different sources of ^{10}Be and ^{9}Be (rainfall vs. mineral weathering) and short residence time (You et al., 1989). As such, ^{10}Be(meteoric)/^{9}Be ratios may not faithfully record denudation processes over 10^2–10^3 yrs. Previous studies have suggested that amorphous oxyhydroxides likely form by exchange with dissolved Be at a late stage in soils or rivers, whereas crystalline oxyhydroxides presumably form from amorphous oxyhydroxides aged during pedogenesis where they incorporated Be at an earlier stage (Dannhaus et al., 2018; Wittmann et al., 2015). Hence different reactive phases may record erosion and weathering processes integrating over different temporal scales and sometimes differ from each other in one sample (Wittmann et al., 2015). In contrast, an agreement in ^{10}Be(meteoric)/^{9}Be ratios between different chemical fractions may indicate a residence time of the reactive secondary minerals long enough for homogenization of Be isotopes in the location where reactive fractions form. Indeed, the residence time of hundreds of years for Liwu soils (Hemingway et al., 2018) will likely result in equilibrium of both isotopes, evidenced by the general agreement between ^{10}Be(meteoric)/^{9}Be ratios of the three fractions in the mainstem samples (Figure 3). Hence, we consider that the extremely high D_{met} is unlikely to be caused by a methodological bias. Instead, such D_{met} is caused by specific geological processes in the Liwu Basin, explored in Section 5.4.

To further illustrate the variability in denudation rates in the Liwu Basin, we compare our D_{met} to published rate estimates in the Liwu River integrating over different temporal and spatial scales (Figure 5). Our D_{met} data from the Waheir River (8.0–8.3 mm/yr) fall within the range of local channel incision rates (6.3–12.0 mm/yr) (Dadson et al., 2003). In the Dasha River the *in situ* ^{10}Be-derived rate (D_{insitu} = 5.0 ± 1.8 mm/yr) (Derrieux et al., 2014) agrees, within uncertainty, to sample DS-2 with a D_{met} of 5.5 ± 1.3 mm/yr. We attributed the much higher D_{met} of 21.5 ± 8.0 mm/yr measured for DS-3 (Figure 5) to the larger contribution of storm-triggered landslide materials given that it was collected from flood deposits (Table 2). Such discrepancy between samples collected at one station can occur given the poor sediment mixing in the Liwu Basin (Deng et al., 2019). For the Shakadang River mainly draining marble, our D_{met} (3.4 ± 0.7 mm/yr) is ~2-fold higher than D_{insitu} (1.5 ± 0.4 mm/yr). The large difference between both cosmogenic nuclide-based approaches could be caused by the absence of quartz in large parts of this sub-catchment that might result in a non-representative D_{insitu}. In the mainstem, rate estimates from thermochronology and *in situ* ^{10}Be are much lower than D_{met}. Note, however, that the Central Range of Taiwan has gone through two stages of uplift, including the initial one (∼6 to ∼1 Ma) with slow uplift of ∼1 mm/yr and a second one (since ∼1 Ma) with rapid uplift of 4–10 mm/yr (Lee et al., 2006). As such, denudation rates integrating over centennial-millennial scales should be higher than the million-year scale exhumation rate here derived from a pooled age of 3.1 Ma using thermochronology (Fellin et al., 2017). The upper limits of published basin-wide and local rates in the mainstem are given by the decadal-scale sediment yield (15.8 ± 4.0 mm/yr) (Dadson et al., 2003) and a millennial-scale gorge incision rate (26.0 ± 3.0 mm/yr) (Schaller et al., 2005). Both rates might be overestimated due to potential invalidity of method-specific assumptions: the monthly weighted-average method applied for calculation of gauging-derived sediment yield may be biased by the higher sampling frequency in flood seasons (Kao et al., 2005) and the calculation of gorge incision rate does not take into account lateral gorge wall retreat (Schaller et al., 2005). In comparison, D_{met} in the mid-lower reaches (LW1 and LW2) agree with such literature limits when taking uncertainties into account, and D_{met} at LW3 (>30 mm/yr) are slightly higher (Figure 5).

5.4. Impact of Bedrock Landslides on Large Variability in Denudation Rates

In each sampled sub-basin along the mainstem (from LW3 to LW1), hydrological, topographical, and lithological controlling factors of centennial-millennial scale denudation (Lague, 2014) show very similar basin-averaged metric values (Table 2). We would thus expect denudation rates to agree between methods. However, our observations on D_{met} and denudation/erosion rates from other methods (Figure 5) clearly indicate that this is not the case. Previous studies attributed extremely high denudation rates (or low [^{10}Be]) and the lack of a clear spatial pattern to stochastic events such as recent landslides (Sosa Gonzalez et al., 2017; West et al., 2014) and/or short-term changes in sediment mixing due to hydrological variability (Lupker et al., 2012). Indeed, landslides triggered by heavy storms play an important role in sediment production and transport processes of the Liwu Basin (Hovius et al., 2000; Kuo & Brierley, 2013, 2014). Modeling of the impact of landslides on cosmogenic nuclide concentrations (Niemi et al., 2005; Yanites et al., 2009) suggested that only if the drainage area exceeds e.g., ∼100 km^2, spatially averaged denudation rates from cosmogenic nuclides can be representative even affected by landslides. However, such an averaging effect is also modulated by the efficiency of fluvial sediment mixing (Yanites et al., 2009). Our previous study on the Zhuoshui River in West Taiwan that is also affected by landsliding showed a consistent downstream trend in D_{met} (Deng, Yang, et al., 2020), in contrast to the lack of spatial pattern in the Liwu River. One hypothesis for such discrepancy is that the impact of stochastic landslides may be averaged-out more efficiently in the Zhuoshui River given its favorable conditions of sediment mixing including a larger drainage area (3×10^3 km^2) and wider channels (proportional to drainage area) (Yanites & Tucker, 2010). In comparison, the smaller Liwu Basin is characterized by faster sediment transfer and poorer sediment mixing (Deng et al., 2019) and the sediment sourced from landsliding materials may not be mixed to a representative average. We thus propose that variable contributions of recent landslides (timescale of e.g., 10^0–10^1 yrs), together with poor fluvial sediment mixing, are likely the main geological cause for the extremely high and spatially variable denudation rates observed from multiple methods in the Liwu mainstem (Figure 5). Next we estimate the impact of such landsliding on D_{met}.

Compared to small landslides that only mobilize soil and occur at a high frequency, landslides mobilizing bedrock occur at a deeper depth and commonly contribute most of landsliding materials (Hovius et al., 1997; Marc et al., 2018). Bedrock landslides carry negligible amounts of reactive ^{10}Be (with concurrent extremely low $(^{10}Be/^{9}Be)_{reac}$) as their depth is much deeper than the shallow ^{10}Be infiltration depth scaling with soil depth (Willenbring & von Blanckenburg, 2010), being 0.2–0.9 m in the Liwu Basin (Hemingway et al., 2018). As a result, incorporating bedrock landslide materials into river sediment will lead to an increase in D_{met}. Hence, we first assess the spatial pattern of landslide activity using published results of landsliding mapping, and then model how much bedrock material from landsliding is potentially incorporated into river sediment.

There is a clear downstream gradient in landslide activity, with the majority of the total landslide-affected area (50%) in the whole basin occurring in the fragile slate of the Liwu headwaters (Kuo & Brierley, 2014). In the sampled mid-lower mainstem (LW3 to LW1), a minor landslide-affected area of 0.045 km^2 was identified, accounting for only 2.8% of the total landslide-affected area in the whole Liwu trunk stream (Kuo & Brierley, 2013). Hence, the contribution of landslide debris to all the mainstem locations is mainly sourced from the same unsampled upper reaches, that is, upstream of LW3. Furthermore, based on the average area of individual landslide scars in the upstream of LW3 (Kuo & Brierley, 2013) and an empirical landslide depth-area relationship (Larsen et al., 2010), we roughly estimate an average landslide depth of ∼4.8 m. This depth value estimated from mean landslide area may be overestimated, but it indeed falls within the range of scar depths estimated from other landslides in Taiwan (Marc et al., 2021) and is much deeper than the soil depth in the Liwu Basin.

To quantify the impact of bedrock landsliding on observed mainstem D_{met}, we followed the framework developed by Yanites et al. (2009). We conceptually define sources of each sediment sample as a mixture of soil and bedrock, where soil is eroded from hillslopes by soil creep or small shallow landslides at a mean background rate (D_b, kg/m^2/yr) and fresh bedrock debris is supplied by event-triggered bedrock landslides. This mixing ratio will set the sediment ^{10}Be(meteoric)/^{9}Be ratio and hence D_{met}, as this isotope ratio decreases from a high value in the upper soil to a value close to zero in unweathered bedrock at depth (Maher & von Blanckenburg, 2016). The simplified equation to calculate modeled denudation rates (D_{model}) under the framework of soil-bedrock mixing is based on the dilution effect of fresh landsliding materials on ^{10}Be and as follows:

$$D_{\mathrm{model}} = \frac{D_b}{1 - f_{\mathrm{bedrock}}} \tag{4}$$

where f_{bedrock} is the fractional contribution of sediment mass from bedrock produced by landslides. To constrain basin-averaged soil D_{b} for the Liwu River, we adopted background erosion rates calculated by Chen et al. (2019) from the two catchments closest to the topographic steady-state zone where the Liwu Basin is also located (Chen & Willett, 2016). These yield an average D_b of ∼0.9 mm/yr for the Danan River and an average ∼1.8 mm/yr for the Chihpen River, that is, a D_b range of 0.9–1.8 mm/yr.

To constrain a realistic range of f_{bedrock} we used radiocarbon (^{14}C) in organic carbon as a soil tracer (Hilton et al., 2008; Kao et al., 2014). Its vertical distribution in soil profiles (decreasing with depth) as well as its transport in rivers (bound to particles) is similar to that of ^{10}Be(meteoric)/^{9}Be. In brief, the organic ^{14}C activity, expressed as the fraction of modern ^{14}C (F_{14_B}), is close to one in the upper soil due to addition of biospheric organic carbon and close to zero at depth due to dominance of petrogenic organic carbon in bedrock (Hemingway et al., 2018). Published F_{14_B} values in the Liwu mainstem determined on samples collected in different years covering three typhoon events (Hilton et al., 2008; Kao et al., 2014) vary within one order of magnitude and from 0.04 to 0.43 ($n = 18$, see Table S5 in Supporting Information S1). We can solve for f_{bedrock} using organic ^{14}C data of Liwu sediments and a soil-bedrock ^{14}C mixing model. This isotopic mixing model, modified from Hemingway et al. (2018), is established based on the mass balance of organic matter content (OC) and ^{14}C activity:

$$f_{\mathrm{soil}} + f_{\mathrm{bedrock}} = 1 \tag{5}$$

$$\mathrm{OC}_{\mathrm{sedi}} = \mathrm{OC}_{\mathrm{soil}} \times f_{\mathrm{soil}} + \mathrm{OC}_{\mathrm{bedrock}} \times f_{\mathrm{bedrock}} \tag{6}$$

$$F_{14_{B-\mathrm{sedi}}} \times \mathrm{OC}_{\mathrm{sedi}} = F_{14_{B-\mathrm{sedi}}} \times \mathrm{OC}_{\mathrm{soil}} \times f_{\mathrm{soil}} + F_{14_{B-\mathrm{bedrock}}} \times \mathrm{OC}_{\mathrm{bedrock}} \times f_{\mathrm{bedrock}} \tag{7}$$

where f_{soil} and f_{bedrock} are fractions of soil and bedrock in a sediment sample and need to be solved for. $\mathrm{OC}_{\mathrm{sedi}}$, $\mathrm{OC}_{\mathrm{soil}}$, and $\mathrm{OC}_{\mathrm{bedrock}}$ are the respective organic matter contents (in %) in sediment samples and end-members of soil and bedrock; $F_{14_{B-\mathrm{sedi}}}$, $F_{14_{B-soil}}$ and $F_{14_{B-bedrock}}$ are the respective fractions of modern ^{14}C in sediment samples and end-members of soil and bedrock. Organic carbon contents and F_{14_B} of the upper soil (A + E horizons) in the Central Range, where the Liwu Basin is located, are compiled from Hemingway et al. (2018) ($n = 14$). Organic carbon contents of bedrock from the major lithological formations of the Liwu Basin (Miocene slate, Eocene slate and Tailuko schist, Figure 1) are compiled from Hilton et al. (2010) ($n = 15$). Average values and standard deviations of both end-members are shown in Table S6 of Supporting Information S1. We performed Monte-Carlo simulations in this mixing model to assess the uncertainty of each end member. We randomly generated 10^6 estimates for sediment mixtures using Equations 5–7 based on end-members of soil and bedrock (Table S6 in Supporting Information S1) and f_{bedrock} ranging from 0% to 100%. For each sediment sample, we calculated the average value and standard deviation of f_{bedrock} from a proportion of all the modeled mixtures that can result in the same organic carbon content and F_{14_B} (within analytical uncertainty) as each sample. The modeling results show that f_{bedrock} and f_{soil} in the Liwu mainstem sediments ($n = 18$) vary from 55% to 97% and from 3% to 45%, respectively (Table S5 in Supporting

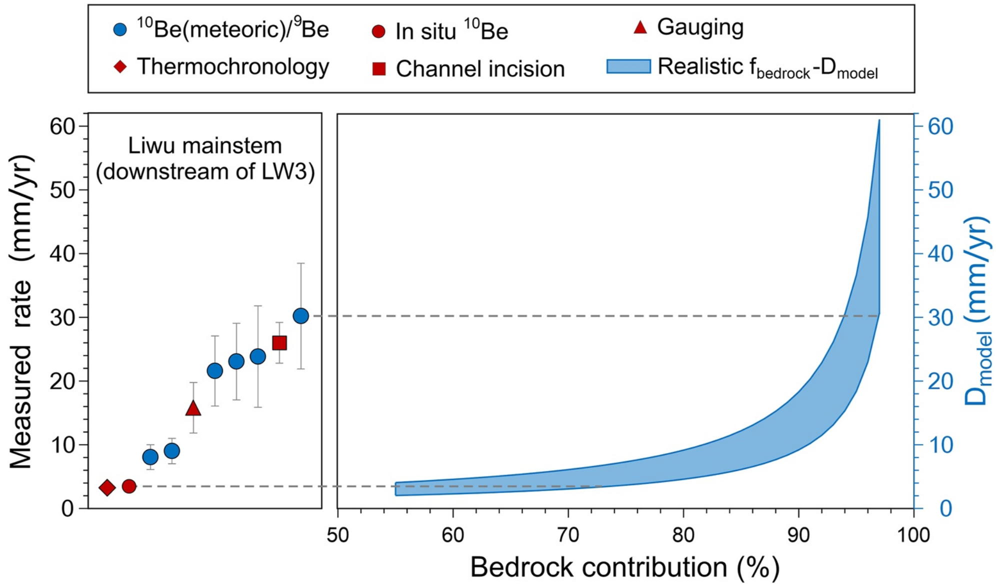

Figure 6. The impact of sediment contribution from bedrock ($f_{bedrock}$) by landslides on modeled denudation rates (D_{model}) in the Liwu River (blue shaded area). D_{met} in the Liwu mainstem (ranging from 8.1 to >30 mm/yr, data from Table 4) are plotted in the left panel, and rate estimates from other approaches are included for comparison. Measured rates are sorted in ascending order. The range of $f_{bedrock}$ (55%–97%) in the Liwu Basin was derived from a soil-bedrock ^{14}C mixing model, while the lower and upper limits of the blue shaded field were constrained using a background soil denudation rate (D_b) range of 0.9–1.8 mm/yr (Chen et al., 2019). Measured D_{met} and other literature data in the Liwu mainstem fall into the range of modeled denudation rates (blue shaded area) based on the soil-bedrock ^{14}C mixing model.

Information S1). In general, the resulting high $f_{bedrock}$ indicates the dominance of contribution of fresh materials, consistent with the measured low F_{14_B} (0.04–0.43) that is closer to the bedrock end-member.

We then calculate the range of D_{model} using modeled $f_{bedrock}$ (55%–97%) according to Equation 4 (Figure 6). All the D_{met} and literature rate estimates obtained for the mainstem fall within the range of D_{model} (Figure 6). Combining the model with D_{met} measurements suggests that bedrock landslides contribute 77%–97% of sediment mass to our mainstem samples (Figure 6). We discount the possibility that D_{met} is biased by this high contribution of bedrock. Such bias potentially arises if sieving has removed coarse-grained materials sourced in bedrock (e.g., pebbles) prior to analysis. Bedrock-rich material adsorbs negligible reactive ^{10}Be and ^{9}Be but contains min ^{9}Be. Although sieving will not affect $(^{10}\mathrm{Be}/^{9}\mathrm{Be})_{reac}$, it might result in an underestimate of $[^{9}\mathrm{Be}]_{min}/[^{9}\mathrm{Be}]_{reac}$ and accordingly of D_{met} in Equation 1. However, we consider this possibility unlikely because the majority of the sediment load is dominated by fine-grained suspended sediment (<63 μm) (Kao et al., 2008; Turowski et al., 2010) and thus our analyzed grain-size is considered to be representative. In brief, variable mixing between soil and bedrock caused by stochastic landsliding can indeed explain the extremely high D_{met} and their large variability in the Liwu mainstem.

These model results are generally applicable to both cosmogenic nuclide methods (*in situ* and meteoric ^{10}Be) as their attenuation with depth is similar, and both methods record a mixture of background denudation rates and landsliding rates (Yanites et al., 2009). Nevertheless, one hypothesis to explain the discrepancy between denudation rates derived from *in situ* ^{10}Be and ^{10}Be(meteoric)/^{9}Be ratios in the mainstem (Figure 5) is the different sensitivity of both methods to the impact of stochastic bedrock landslides. In Taiwan rivers, the majority of the total sediment load including landslide-generated materials is dominated by silt- and clay- sized sediment (Kao et al., 2008; Turowski et al., 2010), similar to the grain-size fraction probed by ^{10}Be(meteoric)/^{9}Be ratios. On the other hand, *in situ* ^{10}Be-derived denudation rates, measured in the coarse sand fraction (e.g., 250–1000 μm, Derrieux et al., 2014) might be mainly derived from coarse-grained and quartz-rich bedrock of minor outcrops and slower denudation, and thus underestimates the impact of rapidly eroding quartz-poor lithologies. In addition, the amount of sediment needed for *in situ* ^{10}Be analysis is extremely large in the Liwu River given the low quartz content and low ^{10}Be concentrations. For example, based on the blank level of *in situ* ^{10}Be analysis reported in Derrieux et al. (2014), bulk sediment grain-size data (Deng et al., 2019), and a gauging-derived sediment yield of 15.8 mm/yr (Dadson et al., 2003), we calculate that to obtain a sufficient amount of quartz in the grain-size fraction of 250–1000 μm such that ^{10}Be amounts exceed the detection limit set by the ^{10}Be blank, a sediment amount exceeding 4.4 kg is needed (details in Table S7 of Supporting Information S1). Hence, denudation rates of >10 mm/yr from *in situ* ^{10}Be are likely below the limit of determination and are thus not accessible for measurements of denudation rates.

As such, the ^{10}Be(meteoric)/^{9}Be proxy may be more suitable in tracing landsliding processes compared to *in situ* ^{10}Be. Although future ^{10}Be(meteoric)/^{9}Be applications in fast-eroding settings should analyze more material (i.e., >2 g of sediment) to further reduce the uncertainties of D_{met}, such required sample amount is still far less than that for *in situ* ^{10}Be method (at least several kg), and does not require labor- and time- intensive mineral separation. Another advantage of ^{10}Be(meteoric)/^{9}Be ratios in fine-grained sediments is that it is more sensitive to landsliding activities as the generated materials may be mostly transported during flood events in the fine-grained, suspended form (Kao et al., 2008; Turowski et al., 2010). Such short-term D_{met} variability may not consistently reflect long-term background denudation, but it can provide detailed information on the style of erosion and its dynamics. For example, given the requirement of several g sediment for ^{10}Be(meteoric)/^{9}Be analysis, we will have the possibility to measure suspended sediments with a high temporal (e.g., hourly) resolution during a typhoon event and record the delivery of storm-triggered landslide materials over event scale and its response to runoff magnitude and variability.

6. Conclusions

We applied the denudation proxy ^{10}Be(meteoric)/^{9}Be ratios to constrain the highest cosmogenic nuclide-derived denudation rates (D_{met}) worldwide, found in the Liwu Basin from the Taiwan orogen, and evaluated how stochastically distributed landslides can affect D_{met}. The major findings are as follows:

(1) We find that the distribution of ^{10}Be(meteoric)/^{9}Be ratios among all samples agrees between the various reactive fractions. Such consistency hints at a residence time of the reactive secondary minerals sufficient to attain equilibrium of Be isotopes with ambient fluids. This equilibration likely took place in the Liwu soil.

(2) D_{met} varies from 8.1 to >30 mm/yr in the Liwu mainstem, and from 3.4 to 21.5 mm/yr in the tributaries. Most of D_{met} in the Liwu Basin agree with literature rate estimates within uncertainty. The extremely fast erosion processes lead to a much lower Be-specific weathering intensity ($f_{reac\text{-}c}$ of ~0.1) than observed in global large river systems (~0.3 on average).

(3) We invoke stochastically distributed landslides to explain the extremely high values (>10 mm/yr) and variability (4-fold) in mainstem D_{met}. Assuming that each sediment sample is a mixture of soil derived from hillslope creep and bedrock mobilized by landslides, we derive a range of fractional contributions of bedrock ($f_{bedrock}$ of 55%–97%) to Liwu mainstem sediments using a soil-bedrock ^{14}C mixing model and a published river particulate organic ^{14}C data set. The measured D_{met} data set agrees with modeled rate estimates by $f_{bedrock}$.

We conclude that the ^{10}Be(meteoric)/^{9}Be proxy can provide geomorphically meaningful constraints on the highest denudation rates in the world even though a few extremely high rates are associated with a large uncertainty. This study sheds new light on the limitations of the determination of cosmogenic-derived denudation rates in landslide-dominated routing systems, and also on the potential of ^{10}Be(meteoric)/^{9}Be in tracing landsliding processes.

Data Availability Statement

GCM-derived ^{10}Be depositional flux data can be accessed online (https://doi.org/10.5880/GFZ.3.4.2015.001).

Acknowledgments
The authors thank Mikael Attal, Odin Marc, Robert Hilton and two anonymous reviewers for their valuable comments. The authors thank Yuan-Pin Chang, James T. Liu, Lei Bi, and Ni Su for supporting the field trip to Taiwan Island and Jens Turowski for providing bedrock samples. The authors thank Steve Binnie and Stefan Heinze from Cologne University for providing AMS measurements. This work was supported by the National Natural Science Foundation of China (Grant No. 41991324, 42006059, and 41730531). K. Deng thanks the Freie Universität Berlin-China Scholarship Council (FUB-CSC) PhD Program for his scholarship in Germany. Open Access funding enabled and organized by Projekt DEAL.

References

Barg, E., Lal, D., Pavich, M. J., Caffee, M. W., & Southon, J. R. (1997). Beryllium geochemistry in soils: Evaluation of 10Be/9Be ratios in authigenic minerals as a basis for age models. *Chemical Geology*, *140*(3), 237–258. https://doi.org/10.1016/S0009-2541(97)00051-X

Blattmann, T. M., Wang, S. L., Lupker, M., Märki, L., Haghipour, N., Wacker, L., et al. (2019). Sulphuric acid-mediated weathering on Taiwan buffers geological atmospheric carbon sinks. *Scientific Reports*, *9*(1), 2945. https://doi.org/10.1038/s41598-019-39272-5

Brown, E. T., Edmond, J. M., Raisbeck, G. M., Bourlès, D. L., Yiou, F., & Measures, C. I. (1992). Beryllium isotope geochemistry in tropical river basins. *Geochimica et Cosmochimica Acta*, *56*(4), 1607–1624. https://doi.org/10.1016/0016-7037(92)90228-b

Bufe, A., Hovius, N., Emberson, R., Rugenstein, J. K. C., Galy, A., Hassenruck-Gudipati, H. J., & Chang, J.-M. (2021). Co-variation of silicate, carbonate and sulfide weathering drives CO_2 release with erosion. *Nature Geoscience*, *14*(4), 211–216. https://doi.org/10.1038/s41561-021-00714-3

Calmels, D., Galy, A., Hovius, N., Bickle, M., West, A. J., Chen, M.-C., & Chapman, H. (2011). Contribution of deep groundwater to the weathering budget in a rapidly eroding mountain belt, Taiwan. *Earth and Planetary Science Letters*, *303*(1–2), 48–58. https://doi.org/10.1016/j.epsl.2010.12.032

Chen, C.-Y., & Willett, S. D. (2016). Graphical methods of river profile analysis to unravel drainage area change, uplift and erodibility contrasts in the Central Range of Taiwan. *Earth Surface Processes and Landforms*, *41*(15), 2223–2238. https://doi.org/10.1002/esp.3986

Chen, C.-Y., Willett, S. D., Joshua West, A., Dadson, S., Hovius, N., Christl, M., & Shyu, J. B. H. (2019). The impact of storm-triggered landslides on sediment dynamics and catchment-wide denudation rates in the southern Central Range of Taiwan following the extreme rainfall event of Typhoon Morakot. *Earth Surface Processes and Landforms*, *45*. https://doi.org/10.1002/esp.4753

Chen, Z. S., Hseu, Z. Y., & Tsai, C. C. (2015). The soils of Taiwan. In *World soils book*.

Chmeleff, J., von Blanckenburg, F., Kossert, K., & Jakob, D. (2010). Determination of the ^{10}Be half-life by multicollector ICP-MS and liquid scintillation counting. *Nuclear Instruments & Methods in Physics Research, Section B, Beam Interactions with Materials and Atoms*, *268*(2), 192–199. https://doi.org/10.1016/j.nimb.2009.09.012

Cook, K. L., Hovius, N., Wittmann, H., Heimsath, A. M., & Lee, Y.-H. (2018). Causes of rapid uplift and exceptional topography of Gongga Shan on the eastern margin of the Tibetan Plateau. *Earth and Planetary Science Letters*, *481*, 328–337. https://doi.org/10.1016/j.epsl.2017.10.043

Dadson, S. J., Hovius, N., Chen, H., Dade, W. B., Hsieh, M.-L., Willett, S. D., et al. (2003). Links between erosion, runoff variability and seismicity in the Taiwan orogen. *Nature*, *426*(6967), 648–651. https://doi.org/10.1038/nature02150

Dannhaus, N., Wittmann, H., Krám, P., Christl, M., & von Blanckenburg, F. (2018). Catchment-wide weathering and erosion rates of mafic, ultramafic, and granitic rock from cosmogenic meteoric ^{10}Be/^{9}Be ratios. *Geochimica et Cosmochimica Acta*, *222*, 618–641. https://doi.org/10.1016/j.gca.2017.11.005

Deng, K., Wittmann, H., Hsieh, M.-L., Yang, S., & von Blanckenburg, F. (2021). Deposition and retention of meteoric ^{10}Be in Holocene Taiwan river terraces. *Quaternary Science Reviews*, *265*, 107048. https://doi.org/10.1016/j.quascirev.2021.107048

Deng, K., Wittmann, H., & von Blanckenburg, F. (2020). The depositional flux of meteoric cosmogenic ^{10}Be from modeling and observation. *Earth and Planetary Science Letters*, *550*. https://doi.org/10.1016/j.epsl.2020.116530

Deng, K., Yang, S., Bi, L., Chang, Y.-P., Su, N., Frings, P., & Xie, X. (2019). Small dynamic mountainous rivers in Taiwan exhibit large sedimentary geochemical and provenance heterogeneity over multi-spatial scales. *Earth and Planetary Science Letters*, *505*, 96–109. https://doi.org/10.1016/j.epsl.2018.10.012

Deng, K., Yang, S., von Blanckenburg, F., & Wittmann, H. (2020). Denudation Rate changes along a fast-eroding mountainous river with slate headwaters in Taiwan from ^{10}Be (Meteoric)/^{9}Be Ratios. *Journal of Geophysical Research: Earth Surface*, *125*(2), e2019JF005251. https://doi.org/10.1029/2019JF005251

Derrieux, F., Siame, L. L., Bourlès, D. L., Chen, R. F., Braucher, R., Léanni, L., et al. (2014). How fast is the denudation of the Taiwan mountain belt? Perspectives from in situ cosmogenic ^{10}Be. *Journal of Asian Earth Sciences*, *88*(1), 230–245. https://doi.org/10.1016/j.jseaes.2014.03.012

Dewald, A., Heinze, S., Jolie, J., Zilges, A., Dunai, T., Rethemeyer, J., et al. (2013). CologneAMS, a dedicated center for accelerator mass spectrometry in Germany. *Nuclear Instruments & Methods in Physics Research, Section B: Beam Interactions with Materials and Atoms*, *294*, 18–23. https://doi.org/10.1016/j.nimb.2012.04.030

Dixon, J. L., & von Blanckenburg, F. (2012). Soils as pacemakers and limiters of global silicate weathering. *Comptes Rendus Geoscience*, *344*(11–12), 597–609. https://doi.org/10.1016/j.crte.2012.10.012

Fellin, M. G., Chen, C.-Y., Willett, S. D., Christl, M., & Chen, Y.-G. (2017). Erosion rates across space and timescales from a multi-proxy study of rivers of eastern Taiwan. *Global and Planetary Change*, *157*, 174–193. https://doi.org/10.1016/j.gloplacha.2017.07.012

Fick, S. E., & Hijmans, R. J. (2017). WorldClim 2: New 1-km spatial resolution climate surfaces for global land areas. *International Journal of Climatology*, *37*(12), 4302–4315. https://doi.org/10.1002/joc.5086

Gaillardet, J., Dupré, B., Louvat, P., & Allègre, C. J. (1999). Global silicate weathering and CO_2 consumption rates deduced from the chemistry of large rivers. *Chemical Geology*, *159*(1–4), 3–30. https://doi.org/10.1016/s0009-2541(99)00031-5

Garzanti, E., & Resentini, A. (2016). Provenance control on chemical indices of weathering (Taiwan river sands). *Sedimentary Geology*, *336*, 81–95. https://doi.org/10.1016/j.sedgeo.2015.06.013

Graly, J. A., Reusser, L. J., & Bierman, P. R. (2011). Short and long-term delivery rates of meteoric ^{10}Be to terrestrial soils. *Earth and Planetary Science Letters*, *302*(3–4), 329–336. https://doi.org/10.1016/j.epsl.2010.12.020

Hartshorn, K., Hovius, N., Dade, W. B., & Slingerland, R. L. (2002). Climate-driven bedrock incision in an active mountain belt. *Science*, *297*(5589), 2036–2038. https://doi.org/10.1126/science.1075078

Heikkilä, U., & von Blanckenburg, F. (2015). *The global distribution of Holocene meteoric ^{10}Be fluxes from atmospheric models: Distribution maps for terrestrial Earth's surface applications*. Germany: GFZ Data Services.

Hemingway, J. D., Hilton, R. G., Hovius, N., Eglinton, T. I., Haghipour, N., Wacker, L., et al. (2018). Microbial oxidation of lithospheric organic carbon in rapidly eroding tropical mountain soils. *Science*, *360*(6385), 209–212. https://doi.org/10.1126/science.aao6463

Hilton, R. G., Galy, A., Hovius, N., Chen, M.-C., Horng, M.-J., & Chen, H. (2008). Tropical-cyclone-driven erosion of the terrestrial biosphere from mountains. *Nature Geoscience*, *1*(11), 759–762. https://doi.org/10.1038/ngeo333

Hilton, R. G., Galy, A., Hovius, N., Horng, M.-J., & Chen, H. (2010). The isotopic composition of particulate organic carbon in mountain rivers of Taiwan. *Geochimica et Cosmochimica Acta*, *74*(11), 3164–3181. https://doi.org/10.1016/j.gca.2010.03.004

Hilton, R. G., Galy, A., Hovius, N., Kao, S.-J., Horng, M.-J., & Chen, H. (2012). Climatic and geomorphic controls on the erosion of terrestrial biomass from subtropical mountain forest. *Global Biogeochemical Cycles*, *26*(3), 1–12. https://doi.org/10.1029/2012GB004314

Hilton, R. G., & West, A. J. (2020). Mountains, erosion and the carbon cycle. *Nature*, *1*(6), 284–299. https://doi.org/10.1038/s43017-020-0058-6

Hohl, S. V., Becker, H., Herzlieb, S., & Guo, Q. (2015). Multiproxy constraints on alteration and primary compositions of Ediacaran deep-water carbonate rocks, Yangtze Platform, South China. *Geochimica et Cosmochimica Acta*, *163*, 262–278. https://doi.org/10.1016/j.gca.2015.04.037

Hovius, N., Stark, C. P., & Allen, P. A. (1997). Sediment flux from a mountain belt derived by landslide mapping. *Geology*, *25*(3), 231–234. https://doi.org/10.1130/0091-7613(1997)025<0231:SFFAMB>2.3.CO;2

Hovius, N., Stark, C. P., Hao-Tsu, C., & Jiun-Chuan, L. (2000). Supply and removal of sediment in a landslide-dominated mountain belt: Central Range, Taiwan. *The Journal of Geology*, *108*(1), 73–89. https://doi.org/10.1086/314387

Huang, C. Y., Yuan, P. B., & Tsao, S. J. (2006). Temporal and spatial records of active arc-continent collision in Taiwan: A synthesis. *The Geological Society of America Bulletin*, *118*(3), 274–288. https://doi.org/10.1130/b25527.1

Kao, S. J., Hilton, R. G., Selvaraj, K., Dai, M., Zehetner, F., Huang, J.-C., et al. (2014). Preservation of terrestrial organic carbon in marine sediments offshore Taiwan: Mountain building and atmospheric carbon dioxide sequestration. *Earth Surface Dynamics*, *2*(1), 127–139. https://doi.org/10.5194/esurf-2-127-2014

Kao, S. J., Jan, S., Hsu, S. C., Lee, T. Y., Dai, M., & Lee, T. Y. (2008). Sediment Budget in the Taiwan Strait with high fluvial sediment inputs from mountainous rivers: New observations and synthesis. *Terrestrial, Atmospheric and Oceanic Sciences*, *19*(5), 525–546. https://doi.org/10.3319/tao.2008.19.5.525(oc)

Kao, S. J., Lee, T. Y., & Milliman, J. D. (2005). Calculating highly fluctuated suspended sediment fluxes from mountainous rivers in Taiwan. *Terrestrial, Atmospheric and Oceanic Sciences*, *16*(3), 653–675. https://doi.org/10.3319/tao.2005.16.3.653(t)

Kuo, C.-W., & Brierley, G. (2014). The influence of landscape connectivity and landslide dynamics upon channel adjustments and sediment flux in the Liwu Basin, Taiwan. *Earth Surface Processes and Landforms*, *39*(15), 2038–2055. https://doi.org/10.1002/esp.3598

Kuo, C.-W., & Brierley, G. J. (2013). The influence of landscape configuration upon patterns of sediment storage in a highly connected river system. *Geomorphology*, *180–181*, 255–266. https://doi.org/10.1016/j.geomorph.2012.10.015

Lague, D. (2014). The stream power river incision model: Evidence, theory and beyond. *Earth Surface Processes and Landforms*, *39*(1), 38–61. https://doi.org/10.1002/esp.3462

Larsen, I. J., Montgomery, D. R., & Korup, O. (2010). Landslide erosion controlled by hillslope material. *Nature Geoscience*, *3*(4), 247–251. https://doi.org/10.1038/ngeo776

Lee, Y. H., Chen, C. C., Liu, T. K., Ho, H. C., Lu, H. Y., & Wei, L. (2006). Mountain building mechanisms in the Southern Central Range of the Taiwan Orogenic Belt—From accretionary wedge deformation to arc–continental collision. *Earth and Planetary Science Letters*, *252*(3), 413–422. https://doi.org/10.1016/j.epsl.2006.09.047

Lupker, M., Blard, P.-H., Lavé, J., France-Lanord, C., Leanni, L., Puchol, N., et al. (2012). ^{10}Be-derived Himalayan denudation rates and sediment budgets in the Ganga basin. *Earth and Planetary Science Letters*, *333–334*, 146–156. https://doi.org/10.1016/j.epsl.2012.04.020

Maher, K., & von Blanckenburg, F. (2016). Surface ages and weathering rates from ^{10}Be(meteoric) and ^{10}Be/^{9}Be: Insights from differential mass balance and reactive transport modeling. *Chemical Geology*, *446*, 70–86. https://doi.org/10.1016/j.chemgeo.2016.07.016

Marc, O., Stumpf, A., Malet, J.-P., Gosset, M., Uchida, T., & Chiang, S.-H. (2018). Initial insights from a global database of rainfall-induced landslide inventories: The weak influence of slope and strong influence of total storm rainfall. *Earth Surface Dynamics*, *6*(4), 903–922. https://doi.org/10.5194/esurf-6-903-2018

Marc, O., Turowski, J. M., & Meunier, P. (2021). Controls on the grain size distribution of landslides in Taiwan: The influence of drop height, scar depth and bedrock strength. *Earth Surface Dynamics*, *9*(4), 995–1011. https://doi.org/10.5194/esurf-9-995-2021

Milliman, J. D., & Farnsworth, K. L. (2011). *River discharge to the coastal ocean—A global synthesis*. Cambridge University Press.

Milliman, J. D., & Syvitski, J. P. M. (1992). Geomorphic/tectonic control of sediment discharge to the ocean: The importance of small mountainous rivers. *The Journal of Geology*, *100*(5), 525–544. https://doi.org/10.1086/629606

Niemi, N. A., Oskin, M., Burbank, D. W., Heimsath, A. M., & Gabet, E. J. (2005). Effects of bedrock landslides on cosmogenically determined erosion rates. *Earth and Planetary Science Letters*, *237*(3), 480–498. https://doi.org/10.1016/j.epsl.2005.07.009

Portenga, E. W., Bierman, P. R., Trodick, C. D., Jr, Greene, S. E., DeJong, B. D., Rood, D. H., & Pavich, M. J. (2019). Erosion rates and sediment flux within the Potomac River basin quantified over millennial timescales using beryllium isotopes. *GSA Bulletin*, *131*(7–8), 1295–1311. https://doi.org/10.1130/B31840.1

Rahaman, W., Wittmann, H., & von Blanckenburg, F. (2017). Denudation rates and the degree of chemical weathering in the Ganga River basin from ratios of meteoric cosmogenic ^{10}Be to stable ^{9}Be. *Earth and Planetary Science Letters*, *469*, 156–169. https://doi.org/10.1016/j.epsl.2017.04.001

Ryan, J. G. (2002). Trace-element systematics of beryllium in terrestrial materials. *Reviews in Mineralogy and Geochemistry*, *50*(1), 121–146. https://doi.org/10.1515/9781501508844-004

Schaller, M., Hovius, N., Willett, S. D., Ivy-Ochs, S., Synal, H. A., & Chen, M. C. (2005). Fluvial bedrock incision in the active mountain belt of Taiwan from in situ-produced cosmogenic nuclides. *Earth Surface Processes and Landforms*, *30*(8), 955–971. https://doi.org/10.1002/esp.1256

Scherler, D., Bookhagen, B., & Strecker, M. R. (2014). Tectonic control on 10Be-derived erosion rates in the Garhwal Himalaya, India. *Journal of Geophysical Research: Earth Surface*, *119*(2), 83–105. https://doi.org/10.1002/2013jf002955

Schwanghart, W., & Scherler, D. (2014). Short Communication: TopoToolbox 2—MATLAB-based software for topographic analysis and modeling in Earth surface sciences. *Earth Surface Dynamics*, *2*(1), 1–7. https://doi.org/10.5194/esurf-2-1-2014

Singleton, A. A., Schmidt, A. H., Bierman, P. R., Rood, D. H., Neilson, T. B., Greene, E. S., et al. (2016). Effects of grain size, mineralogy, and acid-extractable grain coatings on the distribution of the fallout radionuclides ^{7}Be, ^{10}Be, ^{137}Cs, and ^{210}Pb in river sediment. *Geochimica et Cosmochimica Acta*, *197*, 71–86.

Sosa Gonzalez, V., Schmidt, A. H., Bierman, P. R., & Rood, D. H. (2017). Spatial and temporal replicability of meteoric and in situ 10Be concentrations in fluvial sediment. *Earth Surface Processes and Landforms*, *42*(15), 2570–2584. https://doi.org/10.1002/esp.4205

Tsai, H., Maejima, Y., & Hseu, Z. Y. (2008). Meteoric ^{10}Be dating of highly weathered soils from fluvial terraces in Taiwan. *Quaternary International*, *188*(1), 185–196. https://doi.org/10.1016/j.quaint.2007.06.007

Turowski, J. M., Rickenmann, D., & Dadson, S. J. (2010). The partitioning of the total sediment load of a river into suspended load and bedload: A review of empirical data. *Sedimentology*, *57*(4), 1126–1146. https://doi.org/10.1111/j.1365-3091.2009.01140.x

von Blanckenburg, F., Belshaw, N. S., & O'Nions, R. K. (1996). Separation of ^{9}Be and cosmogenic ^{10}Be from environmental materials and SIMS isotope dilution analysis. *Chemical Geology*, *129*(1), 93–99. https://doi.org/10.1016/0009-2541(95)00157-3

von Blanckenburg, F., & Bouchez, J. (2014). River fluxes to the sea from the ocean's Be-10/Be-9 ratio. *Earth and Planetary Science Letters*, *387*, 34–43. https://doi.org/10.1016/j.epsl.2013.11.004

von Blanckenburg, F., Bouchez, J., & Wittmann, H. (2012). Earth surface erosion and weathering from the Be-10 (meteoric)/Be-9 ratio. *Earth and Planetary Science Letters*, *351*, 295–305. https://doi.org/10.1016/j.epsl.2012.07.022

West, A. J., Hetzel, R., Li, G., Jin, Z., Zhang, F., Hilton, R. G., & Densmore, A. L. (2014). Dilution of ^{10}Be in detrital quartz by earthquake-induced landslides: Implications for determining denudation rates and potential to provide insights into landslide sediment dynamics. *Earth and Planetary Science Letters*, *396*, 143–153. https://doi.org/10.1016/j.epsl.2014.03.058

Willenbring, J. K., & von Blanckenburg, F. (2010). Meteoric cosmogenic Beryllium-10 adsorbed to river sediment and soil: Applications for Earth-surface dynamics. *Earth-Science Reviews*, *98*(1–2), 105–122. https://doi.org/10.1016/j.earscirev.2009.10.008

Wittmann, H., von Blanckenburg, F., Bouchez, J., Dannhaus, N., Naumann, R., Christl, M., & Gaillardet, J. (2012). The dependence of meteoric Be-10 concentrations on particle size in Amazon River bed sediment and the extraction of reactive Be-10/Be-9 ratios. *Chemical Geology*, *318*, 126–138. https://doi.org/10.1016/j.chemgeo.2012.04.031

Wittmann, H., von Blanckenburg, F., Dannhaus, N., Bouchez, J., Gaillardet, J., Guyot, J. L., et al. (2015). A test of the cosmogenic ^{10}Be(meteoric)/^{9}Be proxy for simultaneously determining basin-wide erosion rates, denudation rates, and the degree of weathering in the Amazon basin. *Journal of Geophysical Research: Earth Surface*, *120*(12), 2498–2528. https://doi.org/10.1002/2015JF003581

Wobus, C. W., Crosby, B. T., & Whipple, K. X. (2006). Hanging valleys in fluvial systems: Controls on occurrence and implications for landscape evolution. *Journal of Geophysical Research*, *111*(F2). https://doi.org/10.1029/2005jf000406

Yanites, B. J., & Tucker, G. E. (2010). Controls and limits on bedrock channel geometry. *Journal of Geophysical Research*, *115*(F4). https://doi.org/10.1029/2009jf001601

Yanites, B. J., Tucker, G. E., & Anderson, R. S. (2009). Numerical and analytical models of cosmogenic radionuclide dynamics in landslide-dominated drainage basins. *Journal of Geophysical Research*, *114*(F1). https://doi.org/10.1029/2008JF001088

You, C. F., Lee, T., Brown, L., Shen, J., & Chen, J. C. (1988). Be-10 Study of Rapid Erosion in Taiwan. *Geochimica et Cosmochimica Acta*, *52*(11), 2687–2691.

You, C. F., Lee, T., & Li, Y. H. (1989). The partition of Be between soil and water. *Chemical Geology*, *77*(2), 105–118. https://doi.org/10.1016/0009-2541(89)90136-8

References From the Supporting Information

Bierman, P. R., Caffee, M. W., Davis, P. T., Marsella, K., Pavich, M., Colgan, P., et al. (2002). Rates and timing of earth surface processes from in situ-produced cosmogenic Be-10. *Reviews in Mineralogy and Geochemistry*, *50*(1), 147–205. https://doi.org/10.2138/rmg.2002.50.4

Hilton, R. G., Galy, A., Hovius, N., Horng, M.-J., & Chen, H. (2010). The isotopic composition of particulate organic carbon in mountain rivers of Taiwan. *Geochimica et Cosmochimica Acta*, *74*(11), 3164–3181. https://doi.org/10.1016/j.gca.2010.03.004

Lan, C. Y., Lee, C. S., Shen, J. S., & Chia-Yu, L. U. (2002). Nd-Sr isotopic composition and geochemistry of sediments from Taiwan and their implications. *Western Pacific Earth Sciences*, *2*(2), 205–222.

Resentini, A., Goren, L., Castelltort, S., & Garzanti, E. (2017). Partitioning sediment flux by provenance and tracing erosion patterns in Taiwan. *Journal of Geophysical Research: Earth Surface*, *122*(7), 1430–1454. https://doi.org/10.1002/2016JF004026